# 博士論文

# Theory of density-dependent transport on networks

(ネットワーク上における密度依存輸送の理論)

江崎　貴裕

# Contents

# List of Figures

# Chapter 1

# Introduction

## 1.1 Preface

Transportation on networks plays an essentially prerequisite role in our social activities. Efficient network structures enable goods supply [1–3], information communication [4, 5], and human mobility [6–16] in a vast human society. However, as a drawback of this efficiency, its structural complexity often causes breakdowns of the systems [17–20]. In particular, functions of traffic networks (e.g. air traffic networks and road traffic networks [8]) is often impeded by traffic concentration (Fig. 1.1), whose impact could be huge. For instance, the economic impact of traffic jams in Japan reaches 11 trillion yen [21]. Thus, understanding and controlling such jams are vitally important.

The physics of traffic has been studied for decades, disclosing jamming phase transitions in traffic [22, 23] as many-particle systems. In the presence of a jamming state, average flow, defined by a product of the density and velocity of particles, displays a unimodal behavior for the density variation. However, the knowledge is still restricted to simple systems with, for example, ideally uniform roads and uniform particles. By postulating these assumptions, previous studies have revealed a rich structure behind the systems. Their main focus was to understand the macroscopic behavior of the system from the microscopic properties of particles, which is the very tradition of statistical physics. In this thesis I attempt to understand the *macroscopic* behavior (in an entire network) starting from *microscopic* properties of subsystems (Fig. 1.2). Through this second coarse graining, it becomes possible to understand what occurs in traffic systems from a network perspective.

The most notable phenomenon in this context is a macroscopic jamming, wherein the concentration of particles in the network is heavily imbalanced, which is difficult to recover spontaneously. This state is spontaneously induced when the average congestion (density) in the networks is higher than a certain level, whereas uniform density distribution is stable in low density situations. Such bifurcation is not observed in a single subsystem (e.g., a road segment or an airport) but appears only when subsystems are connected with each other.

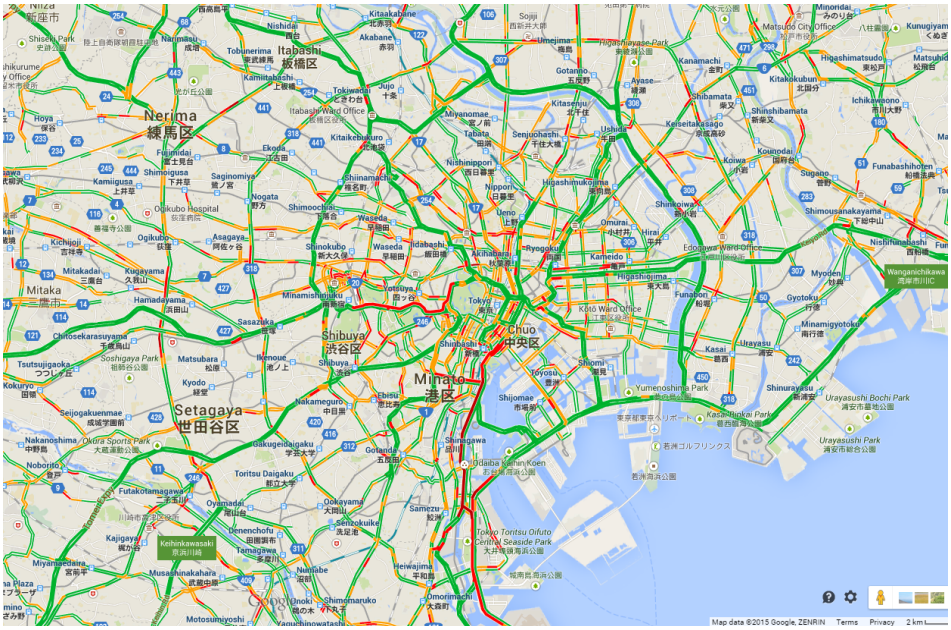


Figure 1.1: Road network in Tokyo [24].

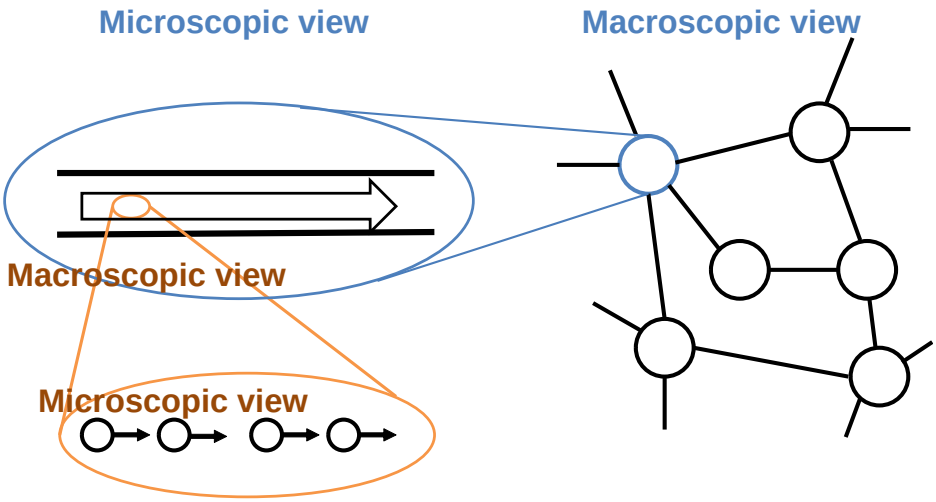


Figure 1.2: Schematic diagram of the second course graining. The relationship on the top (blue) shows a concept in this thesis, whereas the relationship on the left (orange) expresses a conventional concept.

The body of this thesis consists of two parts: (i) the occurrence mechanism and conditions of the macroscopic jam; and (ii) a simple controlling method to mitigate the jamming phenomena. To address this problem, I use a simple model, which assumes the (given) fundamental relationship and equations of continuity. Taking advantage of its mathematical tractability, I attempt to understand these dynamics.

This thesis is organized follows. In the rest of this chapter, I review the background of the *density-dependent* transport and studies on network flow. Chapter 2 defines the model and systems of interest in this thesis. Using the model, first, the local stability of the transportation networks is investigated in Chap. 3. By assuming a piecewise linear fundamental diagram, I study the stability of flow in a chain against large perturbations, as well as the linear stability against small perturbations. Then the results are applied to a route choice problem, and an index for appropriate guidance is shown. In the latter half of Chap. 3, the macroscopic jam is studied in entire networks. I focus on the influence of this jam on macroscopic features of the networks. Based on this knowledge, the U. S. airport networks is investigated, and hints for controlling air traffic efficiently are discussed In Chap. 4. A simple guaranteed solution to the problem is to increase the effective capacity of the system, which is, however, not always feasible in our society confronted by

rapidly increasing traffic demand. Hence, some external control method is necessary to mitigate the jamming phenomenon. Thus, in Chap. 5, a simple controlling method comprised of closure and opening of subsystems is proposed. Even this simple control affects the system significantly, causing three different phases in the system. When the control works efficiently (in the *controlled phase*), the average flow is increased to the level without a macroscopic jam. In contrast, however, when the timings of the opening and closure are inappropriate, the system falls into the *deadlock state*, wherein the traffic is completely frozen. Considering these facts, I discuss the effectiveness of this controlling method. Finally, I conclude the thesis in Chapter 6.

## 1.2 Self-propelled particles

In a recent decades studies in the concept called the self-propelled particles (SPP) systems have been of interest among researchers [22]. SPP is a particle that does not satisfy Newton's third low; such as a car, a human pedestrian, etc. In these systems, the flow of particles is often a quantity of main interest. SPPs interact with each other in many ways. The most fundamental interaction is exclusion; any objects with a "size" cannot occupy exactly the same location. Even if SPPs, such as vehicles, do not collide with each other, they effectively have exclusion force to avoid collisions. Depending on how they exclude or avoid other SPPs, their relationships between flow and density have different properties in detail; however, they all have a simple common characteristic as shown in the next section.

## 1.3 Density-dependent flow

When a system of SPPs is fully occupied by the fluid (imagine, for example, a road fully occupied with cars) its capability for sending flow deteriorates by the congestion (jam). The flow–density relationship is called the "fundamental diagram," which has been vigorously studies in various systems. The idea of the fundamental diagram was first invented for characterizing vehicular traffic flow [25, 26]. To reproduce and understand the empirical fundamental diagrams, numerous studies have been conducted using, for example, car-following models [27–32], cellular automaton models [33–35], and so forth. The idea was later adopted for describing pedestrian flow. The fundamental diagrams for pedestrians have been obtained through experiments [36–43] and observations [44, 45], for

different geometries such as corridors and bottlenecks. In addition to understanding the pedestrian flow, they have been used also for validating pedestrian models [46–50]. Moreover, interestingly, the fundamental diagram has been studied also for ants [51–53]. It is noteworthy that in recent studies [54, 55], the relationship between the number of aircraft on the ground in an airport and the takeoff rate (flow) at that time has been reported. It can also be regarded as the fundamental diagram. In these fundamental diagrams, the effect of congestion is often observed. In this thesis, flow $J$ is described as a function of the particle density, $\rho$:

$$J \equiv J(\rho). \tag{1.1}$$

This function typically has a unimodal shape, comprising of a free-flow phase and a congestion phase [Fig. 1.3(a)]. Essentially this behavior is owing to the exclusion effect of SPPs. In contrast, when the exclusion effect is absent, for example in the presence of a buffer in each location, the fundamental diagram behaves like

$$J(\rho) = \rho v, \tag{1.2}$$

where $v$ is a positive constant, corresponding to the velocity of fluid [Fig. 1.3(b)]. For instance, normal diffusion is categorized in this transportation.

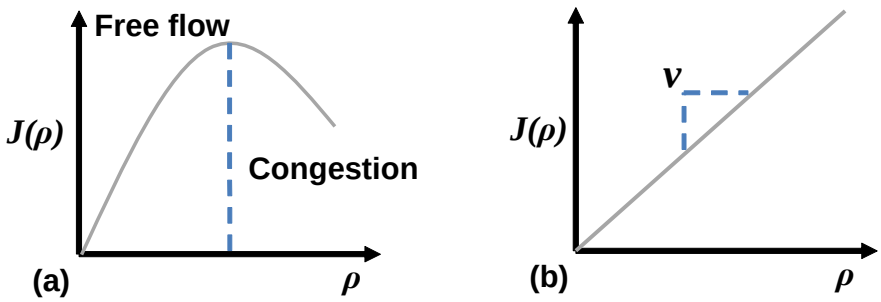


Figure 1.3: Fundamental diagrams of (a) density-dependent transport and (b) density-independent transport.

For the flow of SPPs, the hydrodynamic relationship is written as

$$J(\rho) = \rho v(\rho), \tag{1.3}$$

where $v(\rho)$ defines the functional relationship between the velocity and density of fluid. Normally, $v(\rho)$ is a monotonically decreasing function of the density; that is,

when the system becomes congested, the velocity of particles decreases. Transportation with this density dependence is referred to as the *density-dependent* transport in this thesis. To understand the effect of exclusion on particle flow, it is useful to review the fundamental diagram of the asymmetric simple exclusion process (ASEP) [56, 57], which is the most archetypal model of SPPs transportation, thorough a mean-field treatment. The ASEP is a stochastic process of particles defined on a one-dimensional lattice, comprised of $L$ sites [Fig. 1.4(a)]. The number of particles in the system is denoted by $N$; and thus the density is defined as

$$\rho = \frac{N}{L}. \tag{1.4}$$

Here I assume the periodic boundary; that is, the leftmost and rightmost sites are connected with each other. A particle hops to its right next site if it is empty with rate 1 [Fig. 1.4(a)] [1]. If the site is occupied by a particle, it cannot move (exclusion).

It is known that in the stationary state, every configuration of particles appear with the same probability [56]. As a result, in the thermodynamic limit ($L \to \infty$), the following mean-field approximation exactly predicts the flow in the system. We assume that the probability of finding a particle in a site is $\rho$, and that the correlation between sites are ignorable [Fig. 1.4(b)]. The probability of finding no particle in the next site is given by $1-\rho$. Thus, a particle can hop to the next site with probability $1-\rho$. This *velocity* of a particle decreases as the density increases, because of the shortage of space required for moves. The hydrodynamic equation (1.3) for this system is written as

$$J(\rho) = \rho(1-\rho). \tag{1.5}$$

Thus the unimodal shape [c.f. Fig. 1.3(a)] with a peak at $\rho = \frac{1}{2}$ is obtained.

In vehicular and pedestrian flow, particles decelerate when their headway distance is small. This is due to the effective exclusion effect to avoid collision. It has been known that in these systems, the time-headway (the headway distance divided by the current velocity) is a very important factor [58–60].

It is noteworthy that most of the related studies on transport phenomena on networks conducted so far do not consider this effect because the main focus of these studies has been on epidemics spreading, data packet transport, and power grids that all have no congestion effect.

[1] Here the ASEP with continuous time development is considered. This event occurs with probability $1dt$ in a time interval $dt$.

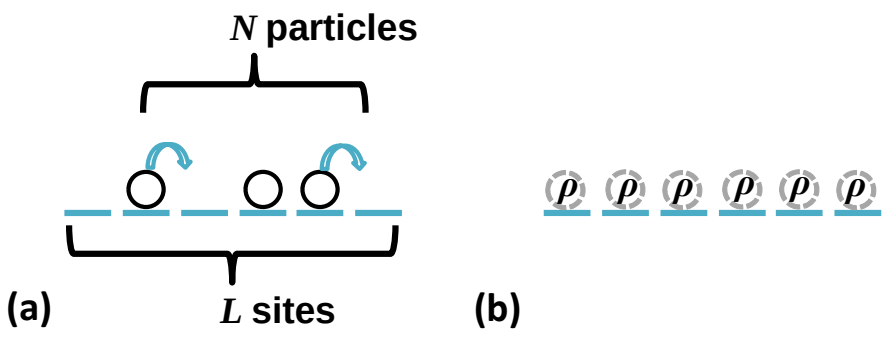


Figure 1.4: (a) Rules of the ASEP. (b) Mean-field approximation.

## 1.4 Network representation

Transportation phenomena on networks have been studied extensively in various fields. They include traffic of data packets on the Internet [61–63], material flow in supply chains [64, 65], epidemic spreading [68, 69] , air [66] and road [7, 67] traffic, etc. Interestingly, this idea is extended even to pedestrian motion in two-dimensional systems [70, 71]. The dynamics in each transport highly depends on its nature. In particular, understanding of dynamics is still limited for *nonlinear* transport systems.

In the frame work presented in this thesis, transport of humans, goods, vehicles, etc. are represented by flow between network nodes. Each node may represent a corresponding element that contains these "fluid" (e.g. a factory, a road segment, or an airport). Links express the connectivity of these nodes, defining the structure of the network, which greatly affects the dynamics of the processes described on it.

In our model, nodes have information of the density of transported objects, which varies according to flow coming in and going out from the nodes with time development.

Here I emphasize the standpoint of the study presented in this thesis. The main interests of the previous studies can be roughly categorized into two; theoretical investigation or computational cost reduction. The first type of studies have analyzed small systems, comprised of two or three nodes, whereas the studies of the second type have effectively simulated the reality or computed scheduling problems. In contrast, the main goal of this thesis is to understand the dynamic

phenomena on networks, such as road network and airport network, on a macroscopic level. Our interest is in how “density dependence” of transport phenomena influences the overall dynamics in networks.

# Chapter 2

# Problem Formalization

In this chapter, I define the focal transport phenomena and a general model for network flow studied in this thesis.

## 2.1 General model

In this chapter I restrict our attention to the following form of transportation on networks. To take the capacity of each node, $c_i$, into consideration, I study normalized density $\rho_i = n_i/c_i$ $(i = 1, \cdots, N)$, instead of particle number in each node. Time development of the density $\rho_i$ is described by the equation of continuity:

$$c_i \frac{d\rho_i}{dt} = \sum_{j=1}^{N} w_{ji} J_j(\rho_j) - \sum_{j=1}^{N} w_{ij} J_i(\rho_i), \tag{2.1}$$

where $w_{ij} \in [0, \infty)$ defines the weight of the link from node $i$ to node $j$. In other words, the output flow from node $i$ determined by $J(\rho_i)$ is allocated to each neighboring site $j$ (when $w_{ij} \neq 0$) as shown in Fig. 2.1. Absence of the link from $i$ to $j$ is expressed as $w_{ij} = 0$. For the sake of simplicity of argument, I assume that the network is strongly connected. [1]

When the system is open, i.e., the total density in the network is not conserved, the above equation can still be used by introducing the nodes representing *density*

[1] A directed network is *strongly connected* if there is a path from node $u$ to $v$ thorough links, for every pair of $(u, v)$. When a network is undirected and strongly connected, it is called the *connected* network. Airport networks and road networks are normally *connected*, or can be divided into connected subnetworks.

*baths*. In these nodes, regardless of flow they receive, the density is kept constant:

$$\frac{d\rho_i}{dt} = 0 \qquad (i: \text{ density bath}). \tag{2.2}$$

Thus they function as constant source and sink of density. They are also useful to consider the behavior of a single node in a network (c.f. Sec. 3.2.1). In the following chapters, I consider closed networks without sink and source nodes, unless otherwise stated.

In practical problems, when a normal node is fully occupied it often rejects flow from neighboring nodes. However, as this rule is problem dependent, I do not impose further rules for the moment.

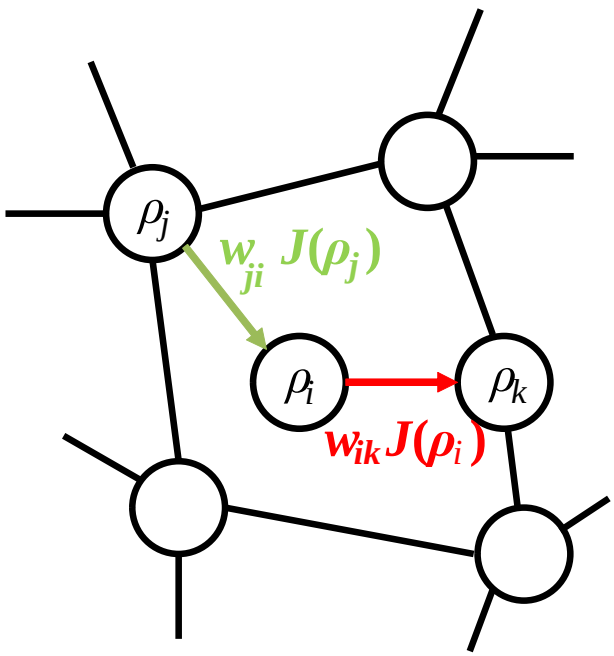


Figure 2.1: Density-dependent flow in a network.

## 2.2 Stationary state

### 2.2.1 Balanced networks

When we consider the density-*independent* transport in which flow is proportional to the density value ($J(\rho) \propto \rho$), the network flow reaches a uniquely possible stationary state [72] in which inflow to and outflow from one node is balanced (Kirchhoff's law). However in our case, the stationary state does not always exist because the flow function $J$ is upper bounded. In this thesis, I restrict myself to considering the *balanced* networks, which is characterized by the following condition,

$$\sum_{j=1}^{N} w_{ji} = \sum_{j=1}^{N} w_{ij}. \tag{2.3}$$

Of course, when the weights are symmetric, i.e., $w_{ji} = w_{ij}$, the network is the balanced network, but in general, the balanced network does not necessarily satisfy this *detailed balanced* condition. The balance network includes two important networks discussed in the following chapters: the first type is an undirected network, i.e., $w_{ij} = w_{ji}$; and the second type is a(n) (unweighted) random regular network in which the indegree and outdegree of nodes are homogeneous.

For the balanced networks, it is obvious that the uniform flow state

$$J_i(\rho_i) = J_0 \qquad (i = 1, \cdots, N) \tag{2.4}$$

can be a stationary solution of Eq. (2.1). The value of $J_0$ is determined though total amount of density in the network for a closed network. Conversely, if the balance condition is not satisfied, the system cannot maintain the homogeneous flow state.

Furthermore, we can also prove the uniqueness of the uniform solution (for a brief proof, see the end of this subsection). Note that, however, this uniqueness does not necessarily mean the uniqueness of the density distribution $(\rho_1, \cdots, \rho_N)$. If the inverse function of $J$ is multivalued, there can be multiple choices of $\rho_i$ for a single $J$ value.

## 2.3 Supplemental information

### 2.3.1 Perron-Frobenius theorem

Let $\mathbf{A}$ be an irreducible $n \times n$ matrix, with non-negative elements $A_{ij} \geq 0$ ($i, j = 1, \cdots, N$). Then, the following statements hold [73]:

(i) $\mathbf{A}$ has a single positive real eigenvalue, which is equal to its spectral radius $\rho(\mathbf{A})$.

(ii) For $\rho(\mathbf{A})$, there exists a positive eigenvector $\mathbf{x}$ whose elements are all positive.

(iii) $\rho(\mathbf{A})$ is a simple eigenvalue of $\mathbf{A}$.

(vi) $\mathbf{x}$ is the only nonnegative eigenvector of $\mathbf{A}$.

(v) $\rho(\mathbf{A})$ satisfies the following inequality:

$$\min_i \left( \sum_{1 \leq j \leq N} A_{ij} \right) \leq \rho(\mathbf{A}) \leq \max_i \left( \sum_{1 \leq j \leq N} A_{ij} \right). \tag{2.5}$$

### 2.3.2 Uniqueness of the stationary state

We confirm the uniqueness of the stationary state by considering the solution of the following balance equation,

$$0 = \sum_{j=1}^{N} w_{ji} J_j - \sum_{j=1}^{N} w_{ij} J_i. \tag{2.6}$$

Using a flow vector $\mathbf{J} = (J_1, J_2, \cdots, J_N)^T$, this equation is written as

$$\mathbf{L}\mathbf{J} = 0, \tag{2.7}$$

where $\mathbf{L}$ is the Laplacian matrix of the focal network, whose elements are defined as

$$\begin{cases} L_{ij} = w_{ij} & \text{(2.8a)} \\ L_{ii} = -\sum_{j=1}^{N} w_{ji}. & \text{(2.8b)} \end{cases}$$

The solution of this equation (2.7) is also an eigenvector of $\mathbf{L}$ corresponding to its eigenvalue $\lambda = 0$. One can find a trivial eigenvector $\mathbf{J_1} = (1, 1, \cdots, 1)^T$, which is equivalent to Eq. (2.4). Thus, now it is sufficient to prove the uniqueness of the eigenvector for the eigenvalue $\lambda = 0$.

Let $W$ denote the minimum orthogonal element of $\mathbf{L}$,

$$W = \min_i \left\{ -\sum_{j=1}^{N} w_{ji} \right\}. \tag{2.9}$$

Then, I define the matrix, $\mathbf{M}$ as

$$\mathbf{M} = \mathbf{L} - W\mathbf{I} = \begin{pmatrix} -\sum_{j=1}^{N} w_{j1} - W & w_{21} & w_{31} & \cdots & w_{N1} \\ w_{12} & -\sum_{j=1}^{N} w_{j2} - W & w_{32} & \cdots & w_{N2} \\ \vdots & \vdots & \ddots & & \vdots \\ w_{1N} & w_{2N} & \cdots & \cdots & -\sum_{j=1}^{N} w_{jN} - W \end{pmatrix}, \tag{2.10}$$

which satisfies the following conditions:

- All the elements of the matrix $\mathbf{M}$ are nonnegative.
- The matrix $\mathbf{M}$ is irreducible (because the focal networks are strongly connected).

Thus we can apply the Perron-Fronbenius theorem (for irreducible matrices; see Sec. 2.3.1) [73] to this matrix. By this theorem, the uniqueness of nonnegative eigenvector $\mathbf{J}$ (whose elements are all nonnegative) is guaranteed. The corresponding eigenvalue is given by $\mu = r(\mathbf{M})$ satisfying

$$\min_i \sum_{j=1}^{N} M_{ij} \leq r(\mathbf{M}) \leq \min_i \sum_{j=1}^{N} M_{ij}. \tag{2.11}$$

Since the lhs and rhs of the inequality are both identical to $-W$, we find $\mu = -W$. From the definition,

$$\mathbf{MJ}(= -W\mathbf{J}) = \mathbf{LJ} - W\mathbf{IJ} = \mathbf{LJ} - W\mathbf{J}. \tag{2.12}$$

Hence, the vector $\mathbf{J}$ is also the eigenvector of $\mathbf{L}$ corresponding to the zero eigenvalue. Thus, the uniqueness of the stationary flow vector has been proved.

If we further impose the detailed balance condition $w_{ij} = w_{ji}$, this uniqueness can be proved using the Courant-Fischer min-max theorem (Sec. 2.3.3).

### 2.3.3 Uniqueness of the stationary state for undirected networks.

When the weight matrix is symmetric, the uniqueness of the eigenvalue corresponding to the zero eigenvalue of $\mathbf{L}$ can be proved without using the Perron-Frobenius theorem. From the definition, $\mathbf{L}$ is a symmetric, real, and irreducible matrix. First, I confirm that $\mathbf{L}$ is semidefinite. For an arbitrary vector $\mathbf{x} \in \mathbb{R}^N$:

$$\mathbf{x}^T\mathbf{L}\mathbf{x} = \sum_{i=1}^{N} x_i \sum_{j=1}^{N} L_{ij}(x_i - x_j) \tag{2.13}$$

$$= \frac{1}{2}\sum_{i=1}^{N}\sum_{j=1}^{N} L_{ij}(x_i - x_j)^2 \geq 0. \tag{2.14}$$

Therefore all the eigenvalues of $\mathbf{L}$, $\lambda_1, \cdots, \lambda_N$ (including duplication), are non-negative, and thus, we can rearrange them as $0 = \lambda_1 \leq \lambda_2 \leq \cdots = \lambda_N$ without loss of generality.

Taking advantage of Courant-Fischer min-max theorem [73], one can evaluate the second smallest eigenvalue as

$$\lambda_2 = \max_{|\mathbf{c}|=1} \min_{\mathbf{c}^T\mathbf{x}=0, \mathbf{x}\neq 0} \frac{\mathbf{x}^T L\mathbf{x}}{\mathbf{x}^T\mathbf{x}} \tag{2.15}$$

$$\geq \min_{\mathbf{J_1}^T\mathbf{x}=0, \mathbf{x}\neq 0} \frac{\mathbf{x}^T L\mathbf{x}}{\mathbf{x}^T\mathbf{x}}. \tag{2.16}$$

Because an vector $\mathbf{x}$ is orthogonal to $\mathbf{J_1}$, it has elements that comprise of at least two different values, $x_i \neq x_j$ $(i \neq j)$. On the other hand, $L$ is an irreducible matrix, and thus the sum Eq. (2.14) must have a term $(x_i - x_j)^2 > 0$. Therefore, the final expression in the above equation must be positive, and $\mathbf{J_1}$ is a unique eigenvector for $\lambda = 0$.

# Chapter 3

# Stability analyses

In the previous chapter, the presence of the uniform stationary state was discussed. Even if the state exists, it could be unstable and unattainable in the system. To understand this instability from a microscopic level, simple systems are studied. First, I investigate the dynamics on a single node with a steady inflow. By considering the behavior of small perturbations added to the uniform stationary state, we can understand the basic mechanism of the destabilization. In addition to this analysis only on small perturbations, large periodic perturbations are also studied. When I assume a piecewise linear fundamental diagram, the systems can be easily integrated, and conditions for preventing a jam is obtained. Using these criteria, I discuss a routing problem. In the presence of a merging of flow, it is important to suppress inflow to one node under the allowable level. Due to the non-monotonic characteristics of the fundamental diagram, the inflow can be controlled by changing the partition ratio of flow in a certain case.

In the latter half of this chapter, the network stability is discussed. The stationary flow is destabilized according to the average density. From a linear stability analysis, we obtain a simple condition for the jamming transition.

## 3.1 Fundamental diagram

First, I define the fundamental diagram of the system (shown in Fig. 3.1) as,

$$J(\rho) = \begin{cases} \frac{j_{\mathrm{cr}}}{\rho_{\mathrm{cr}}}\rho & (0 \le \rho \le \rho_{\mathrm{cr}}), \\ -\frac{j_{\mathrm{cr}}-j_a}{\rho_a-\rho_{\mathrm{cr}}}(\rho-\rho_{\mathrm{cr}}) + j_{\mathrm{cr}} & (\rho_{\mathrm{cr}} < \rho), \end{cases} \tag{3.1}$$

where the dimensionless quantities ($\rho_{\rm cr}$, $j_{\rm cr}$) and ($\rho_a$, $j_a$) correspond to the particle density and flow at the critical point and accommodation limit, respectively. The accommodation limit corresponds to the maximum density that can be achieved in a node. This expression will be used in the latter half of Sec. 3.2.2, and Sec. 3.2.3. Unless otherwise mentioned, we do not specify the fundamental diagram in this chapter. Note that when a node is too congested ($j = j_a$), the aforementioned formulation needs modifications (particle flow will avoid the congested node, which will be discussed in Chap. 5). In this chapter I focus on *avoiding* such a severe jamming and do not consider dynamics after the occurrence of such jamming.

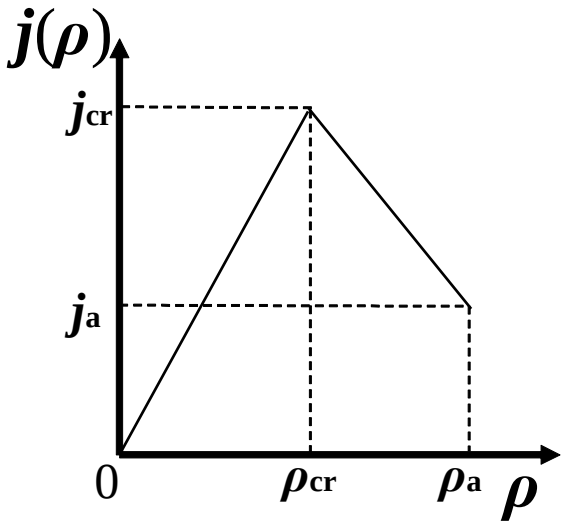


Figure 3.1: Unit fundamental diagram.

## 3.2 Local Stability

### 3.2.1 Stability on a single node

We first consider a single node with a fundamental diagram $J(\rho)$ to which steady inflow, $J(\rho_0)$, is present [Fig. 3.2 (a)]. In this system, $\rho = \rho_0$ is a candidate for the steady state. By considering a slightly perturbed state $\rho = \rho_0 + \epsilon$ ($\epsilon \ll 1$), the

system equation for $\epsilon$ is written as

$$\frac{d\epsilon}{dt} = -J'(\rho_0)\epsilon. \tag{3.2}$$

Here, the abbreviated expression, $J'(\rho_0) \equiv \left.\frac{dJ}{d\rho}\right|_{\rho=\rho_0}$ is used. Thus, if $J'(\rho_0) < 0$, $\zeta$ grows and the state becomes unstable. Note that this region in the fundamental diagram is often associated with *jamming* in a single subsystem. For a unimodal fundamental diagram, obviously $J'(\rho) > 0$ ($\rho < \rho_{\mathrm{cr}}$) and $J'(\rho) < 0$ ($\rho > \rho_{\mathrm{cr}}$). As a result, when the density is smaller than $\rho_{\mathrm{cr}}$, the stationary state can be retained, whereas when nodes are congested, the state is no longer stable and the density increases or decreases depending on the initial value of the perturbations (Fig. 3.3). Once the inflow and outflow are imbalanced and the system becomes congested, it cannot recover the high flow state it had in the free-flow regime. Hence, inflow to a node should be kept lower than its maximum flow capacity, $J(\rho_{\mathrm{cr}})$, to achieve the steady free flow. Note that the inflow may exceed $J(\rho_{\mathrm{cr}})$ temporarily in unsteady states.

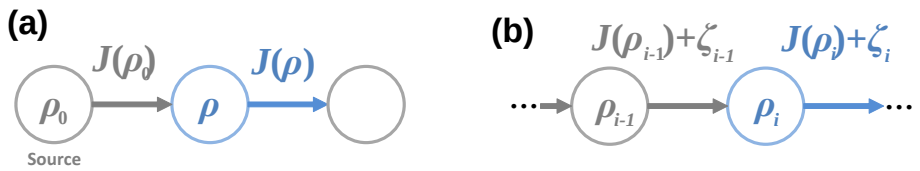


Figure 3.2: Nodes with (a) steady inflow and (b) perturbed inflow.

### 3.2.2 Stability on a chain of nodes

As a simple but important example, I consider a chain of nodes, as depicted in Fig. 3.2 (b). We focus on the dynamics of two successive nodes, whose fundamental diagrams are $J_{i-1}(\rho_{i-1})$ and $J_i(n_i)$, respectively. The required condition for stationary flow is given by

$$J_{i-1}(\rho^*_{i-1}) = J_i(\rho^*_i). \tag{3.3}$$

Since the large density regime, $\rho > \rho_{\mathrm{cr}}$, is unstable (as shown in the previous subsection), I here consider $\rho^*_{i-1}$ and $\rho^*_i$ both being smaller than $\rho_{\mathrm{cr}}$.

In this system, a fluctuation of flow from upstream node $i-1$, $\zeta_{i-1}$, perturbs the density in node $i$, resulting in a fluctuation on its outflow, $\zeta_i$. Here, our interest

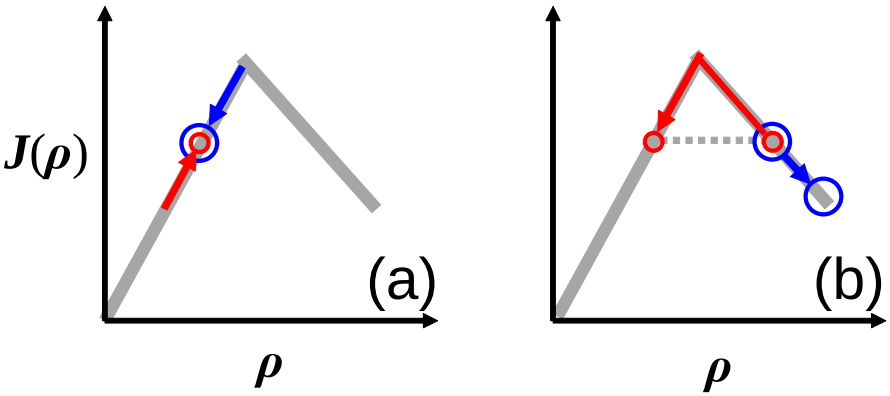


Figure 3.3: Locally (a) stable and (b) unstable behaviors of the system. In the unstable regime, a jam grows with a positive perturbation, whereas it is dissolved by a negative perturbation.

is whether the magnitude of the fluctuation in the inflow is intensified by going through node $i$. Because density flow through a node is often intermittent in reality [74,75] (in other words, it inherently has fluctuations in itself), this type of stability is important for practical applications. The response of the density to the inflow fluctuation is described by

$$\frac{d\epsilon_i}{dt} = -J_i'(\rho_i^*)\epsilon_i + \zeta_{i-1}. \tag{3.4}$$

By expanding $\zeta_{i-1}$ with Fourier modes $A_\omega e^{i\omega t}$ and substituting it into the equation, the response of $\epsilon_i$ to each mode is obtained as

$$\epsilon_i = \frac{A_\omega}{J_i'(\rho_i^*) + i\omega} e^{i\omega t}. \tag{3.5}$$

As a result, compared with the amplitude of fluctuation in the inflow, $\zeta_{i-1}$, the fluctuation in the outflow from node $i$, $\zeta_i$, is reduced by

$$\frac{\left|J_i'(\rho_i^*)\right|}{\sqrt{\omega^2 + J_i'(\rho_i^*)^2}} \tag{3.6}$$

times, which is always smaller than 1. To summarize, small fluctuations of flow that can be described by linear approximation is *not* simply intensified through successive nodes.

Next, I discuss the response of a node against large fluctuations in the inflow by considering a specific fundamental diagram, which is given by Eq. (3.1). Due to its piecewise linearity, the dynamics are still tractable mathematically. In this case, the linearized equation (3.4) can be used by replacing $J_i'(\rho_i^*)$ by $\frac{w_i j_{\mathrm{cr}}}{\rho_{\mathrm{cr}}}$. For a large inflow fluctuation $A_\omega e^{i\omega t}$ (here, $|A_\omega|$ is no longer small), the response of the density in node $i$ is given by Eq. (3.5). When the amplitude of the fluctuation is sufficiently large, density $\rho_i$ might exceed $\rho_{\mathrm{cr}}$, falling into an unstable regime. Thus, a sufficient condition to avoid this can be written as follows:

$$\rho_{\mathrm{cr}} - \rho_i^* > \frac{|A_\omega|}{\sqrt{\omega^2 + w_i^2 j_{\mathrm{cr}}^2/\rho_{\mathrm{cr}}^2}} \tag{3.7}$$

For a given set of $\rho_i^*, \rho_{\mathrm{cr}}, w_i$, and $j_{\mathrm{cr}}$, a stable condition for $A_\omega$ and $\omega$ is depicted in Fig. 3.4. One can see that the system is more stable for high-frequency fluctuations.

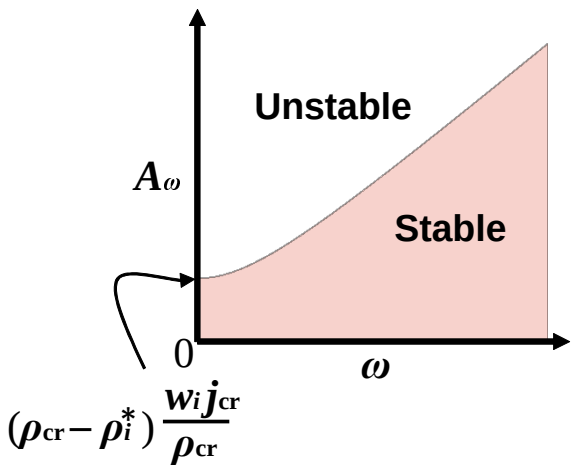


Figure 3.4: Stable conditions with parameters in periodic perturbations, $A$ and $\omega$. For large $\omega$, the boundary increases almost linearly.

### 3.2.3 Node choice and partition problem

We have discussed flow through nodes by ignoring nodes with more than one exit node. These include cases that have a branch and merge leading to an exit (Fig.

3.5). Here, I address this situation from a jam-avoidance perspective. The net flow in this system is determined by flux at the final node [76]. Therefore, it is important to avoid jamming at this point. Although the capacity of the final node should be designed sufficiently large, the flux might exceed the capacity due to blockage of paths leading to other exits due to, for example, accidents . When that occurs, is it possible to control (reduce) particle flux to a desirable level?

For simplicity, I assume that the three nodes all have the fundamental diagrams described by Eqs. (3.1) and that the fundamental diagram of the exit node is given by $J_3 = wJ(\rho)$. The density values in these nodes are defined as $\rho_1, \rho_2$ and $\rho_3$ ($\rho_3 < \rho_{\mathrm{cr}}$). Here, given a total density at stage-A, $\rho_{\mathrm{tot}}$, how should we partition it into $\rho_1$ and $\rho_2$ ($\rho_1 + \rho_2 = \rho_{\mathrm{tot}}$) ? The criterion for *good* partitioning is characterized by flow maximization from node 3 without causing a jam. The total inflow to node 3, $J_{AB}$, is described as

$$J_{AB} = J(\rho_1) + J(\rho_{\mathrm{tot}} - \rho_1). \tag{3.8}$$

To avoid jamming in node 3, I impose the following condition

$$J_{AB} \leq J_3(\rho_{\mathrm{cr}}) = wj_{\mathrm{cr}}. \tag{3.9}$$

If this condition is always satisfied, $\rho_3$ is kept lower than $\rho_{\mathrm{cr}}$, and thus is free from falling to the jamming state.

First, I specify $J_{AB}$ for a given $\rho_{\mathrm{tot}}$. (Because $\rho_1$ and $\rho_2$ are symmetric, I focus on $\rho_1$.) For each region of $\rho_{\mathrm{tot}}$, a different dependence on $\rho_1$ is shown as summarized in Fig. 3.6. In the figure, the fundamental diagram for node 1 is depicted with black lines and, for each $\rho_1$, the fundamental diagram for node 2, $J(\rho_{\mathrm{tot}} - \rho_1)$, is expressed by gray lines (note that the original shape of $J$ is flipped horizontally). Depending on the values specific to the unit fundamental diagram and $\rho_{\mathrm{tot}}$, there are several possible configurations of the two fundamental diagrams ((i)–(vi)). For each case, I obtain the total flux to node 3 (red lines) by adding them together.

By collecting maximum and minimum values in each case, we can draw a fundamental diagram for stage-A (Fig. 3.7). In the middle region, $\rho_{\mathrm{cr}} < \rho_{\mathrm{tot}} < \rho_{\mathrm{cr}} + \rho_a$, there is a finite area between the two lines, meaning that $J_{AB}$ can take various values by tuning $\rho_1$. If $\rho_{\mathrm{tot}}$ is in this regime, we can control $J_{AB}$ within a certain range, not exceeding the capacity limit, Eq. (3.9).

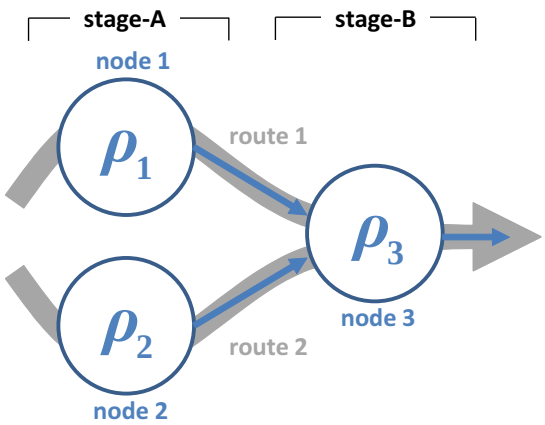


Figure 3.5: Schematic diagram of route choice (at stage-A) and a merging of two paths (at stage-B).

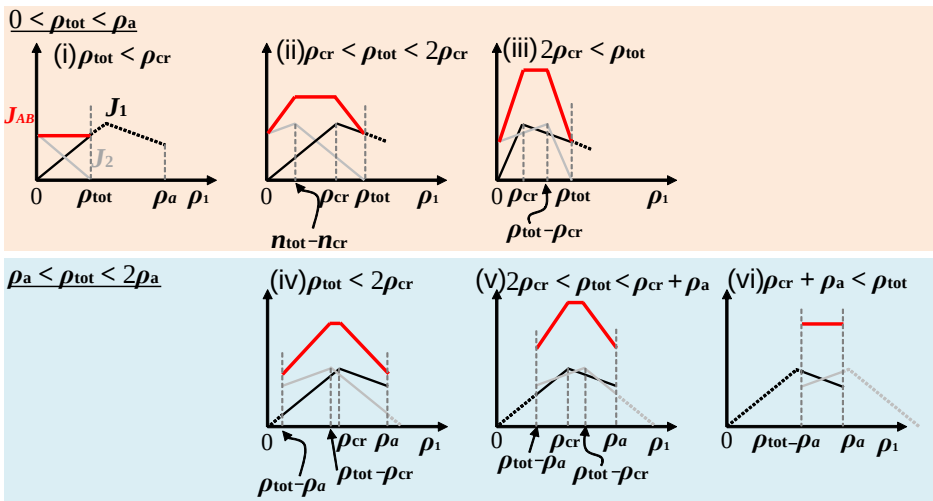


Figure 3.6: Fundamental diagram of the inflow to stage-B for different $\rho_{\text{tot}}$ values. Note that case (iii) occurs when $2\rho_{\text{cr}} < \rho_a$, whereas (iv) occurs otherwise. When $2\rho_{\text{cr}} = \rho_a$, the peaks of the two fundamental diagrams coincide; thus, this point is a boundary of their positional relationship.

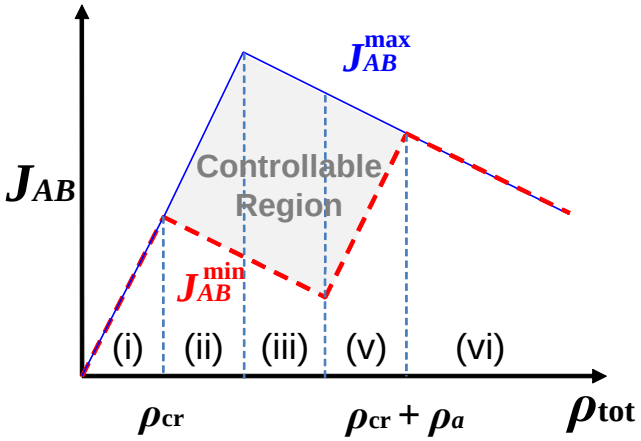


Figure 3.7: Example of the fundamental diagram of flow from stage-A to stage-B (we set $\rho_a = 3\rho_{cr}$ and $j_{cr} = 2j_a$). In the controllable region in the middle, $J_{AB}$ can take any value by tuning $\rho_1$ properly. Note that this diagram is for the case of $2\rho_{cr} < \rho_a$, where case (iv) does not appear (there is no qualitative difference between those of $2\rho_{cr} > \rho_a$).

## 3.3 Network stability

Next, I confirm the presence of a macroscopic jam. For the sake of simplicity, I assume that the fundamental diagrams $J_i$ and capacity of nodes $c_i$ ($i = 1, \cdots, N$) are identical, respectively. Without loss of generality, I specify the capacity as $c_i = 1$.

Consider the state in which density is uniformly distributed in the network, i.e., $\rho_i = \bar{\rho} \quad (i = 1, \cdots, N)$. By linearizing Eq. (2.1) with small perturbations $(\epsilon_1, \cdots, \epsilon_N)^T \equiv \boldsymbol{\epsilon}$ added to this state, we obtain

$$\frac{d}{dt}\boldsymbol{\epsilon} = J'(\bar{\rho})\boldsymbol{L}\boldsymbol{\epsilon}, \tag{3.10}$$

where matrix $\boldsymbol{L}$ is defined by $L_{ij} = w_{ji}$ ($i \neq j$) and $L_{ii} = -\sum_{j=1}^{N} w_{ji} \equiv -W_i$. The state is stable if all the eigenvalues of the matrix, $J'(\bar{\rho})\boldsymbol{L}$, are not positive; strictly speaking, only a single zero eigenvalue is allowed, if any. Otherwise, a small perturbation grows to cause disruptions of flow. First, I prove that the matrix $\boldsymbol{L}$ is negative semidefinite. Let $\boldsymbol{M}$ be the matrix defined by

$$\boldsymbol{M} = \boldsymbol{L} + W^*\boldsymbol{I}, \tag{3.11}$$

where $\boldsymbol{I}$ is the identity matrix and $W^*$ is defined as

$$W^* = \max_{1 \le i \le N} W_i. \tag{3.12}$$

With this additional term, the diagonal elements of $\boldsymbol{M}$ are not smaller than 0. Here, I use the Perron-Frobenius theorem (see Sec. 2.3.1) [73], which gives information about the spectral radius of non-negative irreducible matrices. The spectral radius of the matrix $\boldsymbol{M}$, $\rho(\boldsymbol{M})$, satisfies

$$\min_i \sum_{1 \le j \le N} M_{ij} \le \rho(\boldsymbol{M}) \le \max_i \sum_{1 \le j \le N} M_{ij}. \tag{3.13}$$

From its definition, the left hand side and the right hand side of the inequality are both identical to $W^*$. Thus, the spectral radius is given as $\rho(\boldsymbol{M}) = W^*$, which means eigenvalues of the matrix, $\mu_i$ ($i = 1 \cdots N$), satisfy

$$|\mu_1|, \cdots, |\mu_N| \le W^*. \tag{3.14}$$

The product of the corresponding eigenvectors, $\boldsymbol{x}_i$, and $\mathbf{L}$ yields

$$\boldsymbol{L}\boldsymbol{x}_i = \boldsymbol{M}\boldsymbol{x}_i - W^*\boldsymbol{I}\boldsymbol{x}_i = (\mu_i - W^*)\boldsymbol{x}_i. \tag{3.15}$$

Thus, $\boldsymbol{x}_i$ is an eigenvector of the matrix, $\boldsymbol{L}$, whose corresponding eigenvalue is $\lambda_i = \mu_i - W^*$. Hence, for the eigenvalues of $\boldsymbol{L}$, the conditions

$$|\lambda_1 + W^*|, \cdots, |\lambda_N + W^*| \leq W^* \tag{3.16}$$

are satisfied; that is, they are not positive (see Fig. 3.8).

From the previous arguments, it is obvious that they are all negative when $J'(\bar{\rho}) > 0$ (i.e., $\rho < \rho_{\mathrm{cr}}$). The condition $J'(\bar{\rho}) < 0$ (i.e., $\rho > \rho_{\mathrm{cr}}$) immediately leads to the instability.

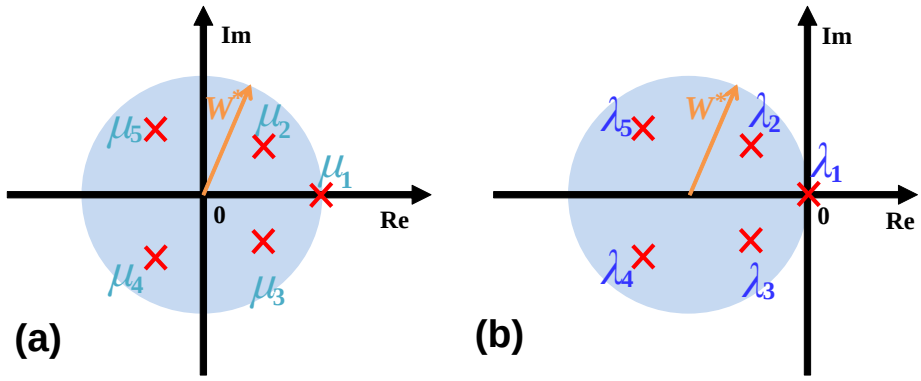


Figure 3.8: Schematic plots of eigenvalues (a) $\mu_i$ and (b) $\lambda_i$ ($i = 1, \cdots, N$).

## 3.4 Summary

I have analytically investigated stability conditions of the network transportation model. From these results, we find two important criteria's to avoid jamming: (i) keep the density in one node less than the critical value of the fundamental diagram by (ii) keeping the inflow to one node (and its fluctuations) smaller than a certain level. Once the system falls into a jamming state, particle flow is significantly restricted by the congested node. To avoid such congestion, inflow to the nodes should be controlled unless their capacities are quite large. The possibility of reducing flow to a desirable level by controlling density is shown using simple examples of density partitions. From arguments based on fundamental diagrams, we find that the total flux can be controlled by changing the partition

ratio when the total density is moderately large. Such a partition could be realized through appropriate guidance (for example, information regarding necessary travel times). It would be useful to integrate such knowledge into the route guidance problem [77–80].

The essence of this fact can be simply phrased as "local congestion ≠ global congestion." Interestingly, this implication applies to granular flow [81] as well as to pedestrian bottleneck flow [82] when an obstacle is placed. An obstacle hinders inflow to the node and reduces the clogging effect of fluid.

# Chapter 4

# Air traffic networks

In this chapter, the model defined in the preceding chapters is applied to the network of airports. Through simulations, I discuss the dynamics air traffic, which can be understood by the degree distribution of the focal network.

## 4.1 Preface

Faced with rapidly growing demand in air traffic, researchers have addressed aggravating congestion problems from various perspectives [83–89]. Airport congestion related to departing aircraft on the ground, i.e., *surface congestion*, is known to be a serious problem, and its relationship to airport performance has been recently investigated [54, 55]. Figure 4.1 shows the empirical takeoff rate at Philadelphia International Airport presented by Simaiakis and Balakrishnan [55]. When the airport is not congested, increasing the number of aircraft on the ground directly leads to a high takeoff rate. However, after the number reaches a critical point, the performance deteriorates due to inefficient aircraft configurations. Thus, this relationship defines a fundamental diagram of the airport.

In this chapter, I aim to disclose the physical aspects of air traffic from the surface congestion viewpoint. For this purpose, I consider a network of airports (nodes), the performance of which is determined by their congestion levels, as shown in Fig. 4.1. Note that network approaches to describe air traffic have been proposed in previous studies [90–92]; however, these studies did not focus on the surface congestion effect. In addition to the conventional approaches in the field of management science, the network modeling of aviation transport has recently been attempted [93, 94] from a network science [95–98] perspective, supported by

the recent understanding of airport networks [12–16]. However, the knowledge of congestion dynamics of air traffic from a network perspective is still limited.

This chapter presents a simple model for aviation transport networks based on the density-flux relationship locally defined in each airport. Our primary goal is to evaluate the stability of global air traffic against disturbances. Because of assumptions imposed in the model, we cannot expect a quantitative description of the real systems. However, taking advantage of its simplicity, I aim to clarify the fundamental features of a spontaneous jam formation.

The remainder of this chapter is organized as follows. The next section defines the model and simulation conditions. In Section 4.3, I show a spontaneous jamming transition phenomenon and its dynamics. Finally, in Section 4.4, I discuss the implication of these phenomena and future works.

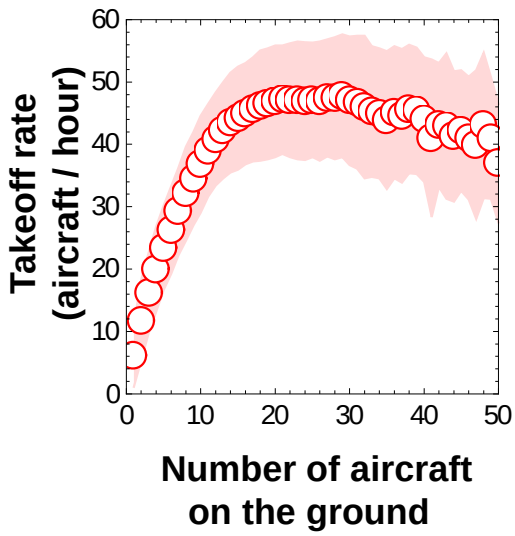


Figure 4.1: Empirical relationship between the takeoff rate and surface congestion at Philadelphia International Airport (Data obtained from Ref. [55].). The shaded area indicates the standard deviation of the data.

## 4.2 Model

### 4.2.1 Problem formulation

Consider $N$ nodes, labeled $1, \cdots, N$, representing each airport. The connectivity of the nodes is defined by an adjacency matrix $\boldsymbol{A}$, whose element $A_{ij}$ indicates the presence ($A_{ij} = 1$) or absence ($A_{ij} = 0$) of a link between the two nodes $i$ and $j$ ($i, j = 1, \cdots, N$). Here, for the sake of simplicity, I assume that each link has an identical capacity. By assuming that each node has a capacity that is proportional to the degree, $k_i = \sum_{j=1}^{N} A_{ij}$, and defining $c_i = k_i$, the time evolution of a density set representing congestion level in each airport, $\{\rho_1, \cdots \rho_N\}$, is written as

$$\frac{d\rho_i}{dt} = \frac{1}{k_i} \sum_{j=1}^{N} A_{ji} J(\rho_j) - J(\rho_i). \tag{4.1}$$

Note that this equation coincides with the general model Eq. (2.1) by defining $w_{ij} = \frac{A_{ij}}{k_i}$.

Note that Sun and Bayen [99] applied this model to air traffic in a different manner, in which nodes correspond to discretized aviation routes.

### 4.2.2 Network geometry

We use $A_{ij}$ defined from the U. S. airport network [100]. The data comprises 500 major airports and 2980 undirected links ($A_{ij} = A_{ji}$), and the network is connected (i.e., there is at least a single path of links between any two different nodes).

In addition, I also use random networks and random regular networks for comparison. The random networks are generated by connecting every pair of nodes with a probability $p$. The number of nodes and the expected number of links are set to be similar to the empirical network; $N = 500$ and $Np = 12$, respectively. The random regular network is the random network with a homogeneous degree distribution. With the fixed number of degree, nodes are connected randomly. The random regular networks are used to discuss the effect of the magnitude of degree, whereas the random networks are used to discuss the difference in the degree of nodes. These random networks do not have specific structure, and thus give neutral references of the system.

### 4.2.3 Fundamental diagram

In this chapter, I define an explicit form of the fundamental diagram as follows:

$$J(\rho_i) = \begin{cases} \rho_i(1-\rho_i) & \text{if } \rho_i < \rho_{\max}, \\ \rho_{\max}(1-\rho_{\max}) & \text{if } \rho_i \geq \rho_{\max}, \end{cases} \tag{4.2}$$

where $\rho_{\max}$ is the maximum density that a single airport can accommodate on the ground. Above this density, aircraft have to stay in the sky near the airport (they still belong to the destination node); $J$ does not decrease since the congestion level on the ground remains the same. Note that in Fig. 4.1, only aircraft on the ground are counted (i.e., $\rho_{\max}$ corresponds to the right end of the figure.). We assumed a quadratic function to describe this part as the simplest smooth unimodal function. This function is often used to model dynamics in which capacity constraints play a role (e.g., vehicular traffic [25], interacting particle systems [57], and population dynamics [101]).

This function is illustrated in Fig. 4.2(a), in which I set $\rho_{\max} = 0.7$. I define the critical density, $\rho_{\mathrm{cr}}$, as the density that gives maximum $J$. In the function (4.2), $\rho_{\mathrm{cr}} = 0.5$.

### 4.2.4 Simulation conditions

At $t = 0$, the initial density of nodes are set almost uniformly as $\bar{\rho}$, which is slightly fluctuated with a random variable $\delta$ drawn from a uniform distribution $[-0.005, 0.005]$. Each simulation is performed until the time development of densities stops. We study the characteristics of the stationary state by investigating key quantities, which will be defined subsequently. Unless otherwise noted, results are averaged over 1000 trials.

## 4.3 Results

### 4.3.1 Global flux–density relationship

I define the global flux, $\bar{J}$, as the average flow per link as follows:

$$\bar{J}(\bar{\rho}) = \frac{\sum_{i=1}^{N}\sum_{j=1}^{N} A_{ij} J(\rho_i^{\infty})}{\sum_{i=1}^{N} k_i}, \tag{4.3}$$

where $\rho_i^\infty$ denotes the density $\rho_i$ in a stationary state. When the density is uniformly distributed in the stationary state, $\bar{J}(\bar{\rho})$ coincides with the local flow $J(\bar{\rho})$ at $t = 0$. However, as illustrated in Fig. 4.2(a), one can find a gap between $\bar{J}(\bar{\rho})$ and $J(\bar{\rho})$ for a certain range of $\bar{\rho}$ due to the nonuniform distribution of $\rho_i^\infty$. For $\bar{\rho} < \rho_{\mathrm{cr}} = 0.5$ and $\bar{\rho} > \rho_{\max} = 0.7$, the uniformity of $\rho_i^\infty = \bar{\rho}$ is conserved for all nodes, whereas for the middle initial density, some nodes take a single constant value of $\rho_i = \rho_l$ while the others distribute in the range of $\rho_i \geq \rho_{\max}$ [Fig. 4.2(b)]. The lower bound density, $\rho_l$, is the density value that satisfies $J(\rho_l) = J(\rho_{\max})$ ($\rho_l < \rho_{\mathrm{cr}}$) [see Fig. 4.3(b)]. Interestingly, at the critical density ($\bar{\rho} = 0.5$), only a small number of nodes draw density from neighboring nodes.

This jamming transition can be understood as a bifurcation phenomenon.

### 4.3.2 Macroscopic jamming transition

Here, I confirm that the network stability is not retained for large density regime as shown in Sec. 3.3. Since the networks discussed in this chapter are all undirected networks, they satisfy the *balance* condition required in the argument in Sec. 3.3.

Therefore, the stability is dependent only on $J'(\bar{\rho})$, i.e., the system is unstable when $J'(\bar{\rho}) < 0$. Thus, *microscopic* jamming in the fundamental relationship $J(\bar{\rho})$ directly triggers a *macroscopic* jam.

The flux deterioration shown in Fig. 4.2(a) can be understood as follows. When the system is not congested [Fig. 4.3(a)], $\rho_i = \bar{\rho}$ is locally stable and the density is uniformly distributed to all nodes. Conversely, in high density cases [Fig. 4.3(b)] this state is no longer stable, and the flow between nodes equilibrates at a lower density value $\rho_i = \rho_l$ and higher density value $\rho_i \geq \rho_{\max}$. Hereafter, I refer to this state as the *macroscopically jamming state*.

### 4.3.3 Global density correlation

In the previous subsection, we found that the density distribution is imbalanced in the macroscopically jamming state. To evaluate the regularity in this stationary density distribution, I define an indicator variable $\gamma_i$, which reflects the density in node $i$:

$$\gamma_i = \begin{cases} 1 & \text{if } \rho_i \geq \rho_{\mathrm{cr}}, \\ -1 & \text{if } \rho_i < \rho_{\mathrm{cr}}. \end{cases} \tag{4.4}$$

Using this variable, correlation between two neighboring nodes is quantified as $A_{ij}\gamma_i\gamma_j$, which returns 1 if two neighboring nodes have the same $\gamma$ and returns

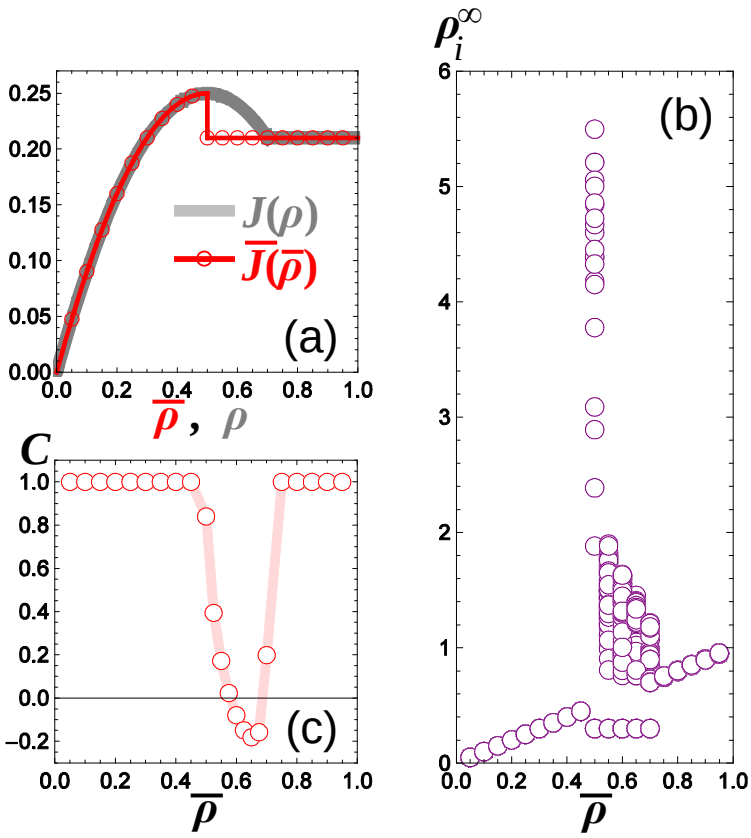


Figure 4.2: (a) Local ($J(\rho)$; gray) and global ($\bar{J}(\bar{\rho})$; red) fundamental diagrams. (b) Stationary density distribution in a single trial. Each circle represents the density in a single node. (c) Global correlation coefficient. When the initial density $\bar{\rho}$ is small and large, all nodes have the same density value, which is reflected in the agreement of the local and global fundamental diagrams [panel (a)]. On the other hand, when $\bar{\rho}$ is in the middle regime ($\rho_l < \bar{\rho} < \rho_{\max}$), the uniformity of the density is broken [panel (b) and (c)], and the global flux is deteriorated [panel (a)].

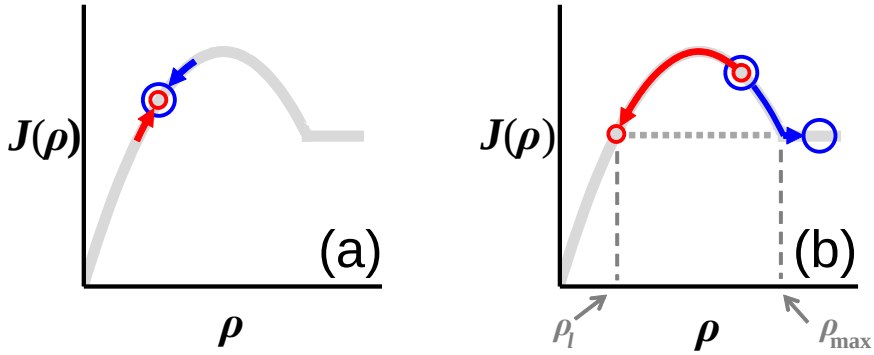


Figure 4.3: Stability of (a) subcritical and (b) supercritical density.

$-1$ otherwise. Figure 4.2(c) illustrates global regularity of the density distribution defined as the average correlation degree per link

$$C = \left\langle \frac{\sum_{i=1}^{N} \sum_{j=1}^{N} A_{ij} \gamma_i \gamma_j}{\sum_{i=1}^{N} k_i} \right\rangle, \tag{4.5}$$

where $\langle x \rangle$ denotes an ensemble average of $x$. Corresponding to the aforementioned bifurcation, $C$ is constant ($C = 1$) for $\bar{\rho} < \rho_{\mathrm{cr}}$ and $\bar{\rho} > \rho_{\mathrm{max}}$, and in the middle density regime, it suddenly decreases to approximately 0, explaining the breakage of the uniform state.

Figure 4.4 shows the global correlation for random regular networks with various $k$ values. When the degree is small, $C$ becomes more smaller, and as the degree increases, the discrepancy between to the results for the random regular and the empirical network becomes small. From these observations, we can conclude that the global regular structure is absent in terms of density correlation in the macroscopically jamming state.

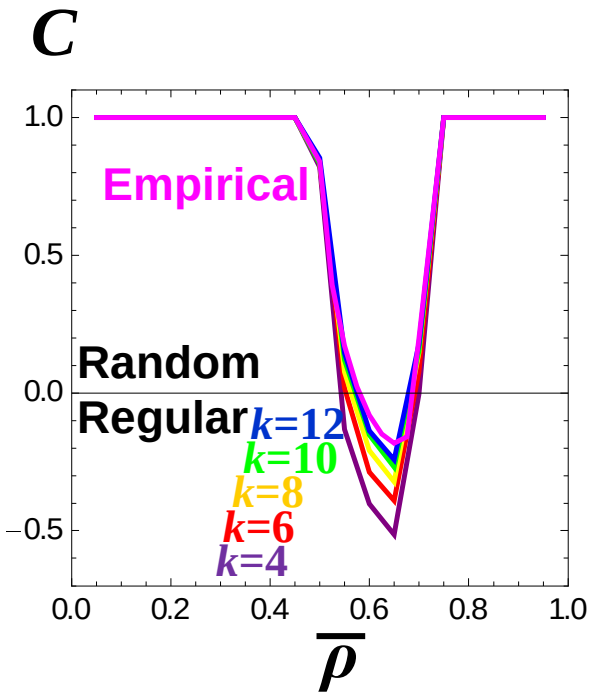


Figure 4.4: Global correlation, $C$, for different network geometries. Figure 4.2(c) is compared with the results for random regular networks with degree $k = 4, 6, 8, 10$, and 12.

### 4.3.4 Local density correlation and dynamics

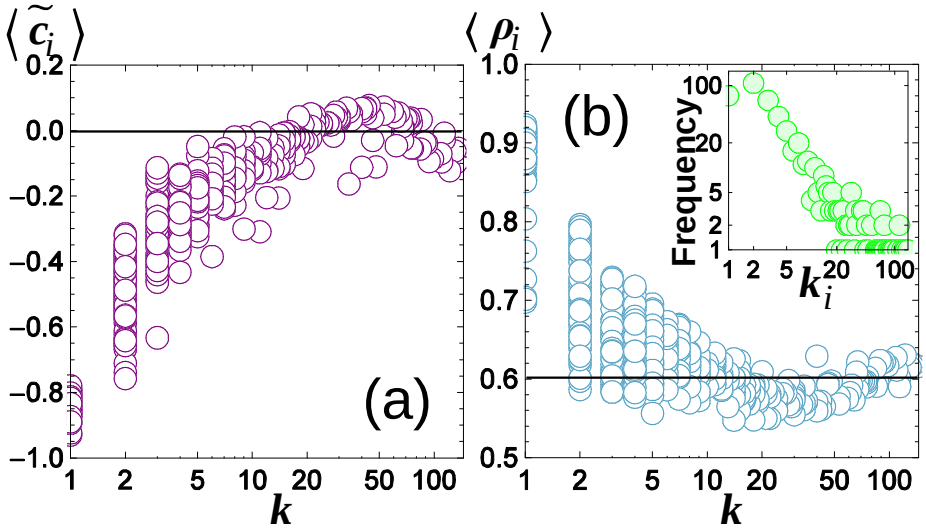


Figure 4.5: (a) Local correlation coefficient. (b) Average density distribution. Each plot corresponds to averaged stationary density in one node. The inset in panel (b) shows degree distribution of the focal network.

Next, I focus on the local regularity of the stationary density distribution. Here, I set $\bar{\rho} = 0.6$ and investigate the average local correlation per node

$$\tilde{c}_i = \left\langle \frac{\sum_{j=1}^{j=N} A_{ij}\gamma_i\gamma_j}{k_i} \right\rangle. \tag{4.6}$$

As shown in Fig. 4.5(a), $\tilde{c}_i$ is highly dependent on $k_i$. Decreasing values of $k$ correspond to values of $\tilde{c}_i$ decreasing to near $-1$, which indicates that a node tends to have an opposite $\gamma$ against its neighboring nodes with high probability. However, as the number of neighboring nodes increases, it becomes difficult to take the opposite value against all the neighboring nodes, and thus the local correlation vanishes. In other words, the presence of high-degree nodes reduces the absolute value of the local and global correlations in the macroscopically jamming state. This is also supported by the results for random regular networks [see Fig. 4.6 displaying $\tilde{c}_i$ for random regular networks (and the random network with $Np = 12$,

which will be mentioned later)]. The local correlation $\tilde{c}_i$ increases according to the degree. It even reaches more than 0 because the average density set in as the initial density is larger than 0.5.

In addition, the density also depends on $k_i$ [Fig. 4.5(b)]. In hub nodes (large nodes), the average density is approximately 0.6, which coincides with $\overline{\rho}$, whereas in nodes with small $k_i$ (small nodes), the average density is significantly larger. This can be explained by the effective relaxation speed of the density [Figs. 4.7(a) and (b)]. This dependency is supported by Fig. 4.7(b), which shows the average of saturation time $T_i = \min\{t|\rho_i(t+1) = \rho_i(t)\}$. This is because, for a large node, the density inflow to the node is averaged over a large number of neighboring nodes and its speed of variation is relatively slow. Therefore, at the beginning of each simulation trial in the middle density regime, the change in density is dominant in small nodes, which is strongly influenced by the initial perturbation $\delta$: for positive $\delta$, the density starts to increase, and for negative $\delta$ density start to decrease. Thus, one half of the small nodes become congested and the other half loses density. Since the drag of density is faster than discharge [Fig. 4.7(a)], and there is no upper limit on the density, the average final density in small nodes becomes large. Conversely, in large nodes, at the beginning, it tends to be deprived of density neighboring small nodes, which leads to a less probability of congestion occurring in these nodes. As a result, the density in large nodes is suppressed.

In addition, in large nodes, $\tilde{c}_i$ and $\rho_i$ slightly decreases and increases, respectively. This seems to stem from the difference in node degree. As can be observed in Fig. 4.6, $\tilde{c}_i$ monotonically increases for random regular networks. However, for a random networks with various $k$'s, it has a peak in the large density regime. In the largest nodes, the time scale of dynamics is particularly slow, and thus they are less affected by neighboring nodes.

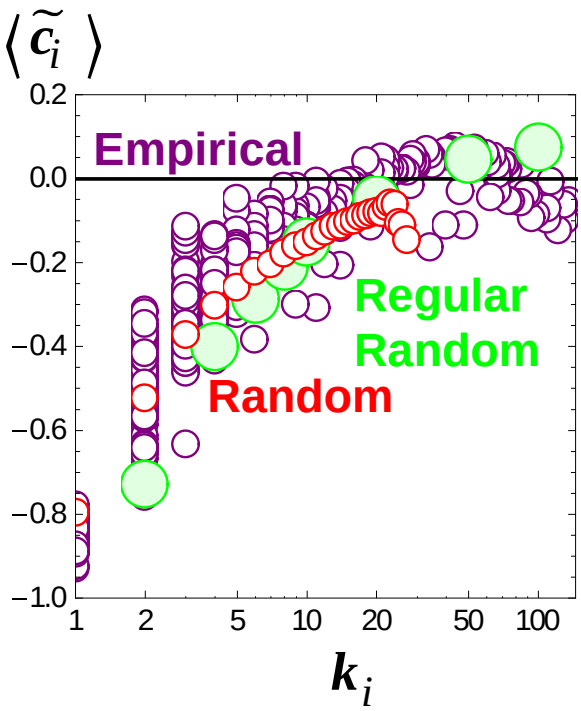


Figure 4.6: Local correlation, $c_i$, for different network geometries. Figure 4.5(a) is compared with the results for random regular networks for different $k$ values (green large circles), and the results for the random network with average degree $Np = 12$ (red small circles) that corresponds to the average degree in the empirical network. The results for the random and random regular networks were averaged over 1000 trials. In both simulations, I set $\bar{\rho} = 0.6$.

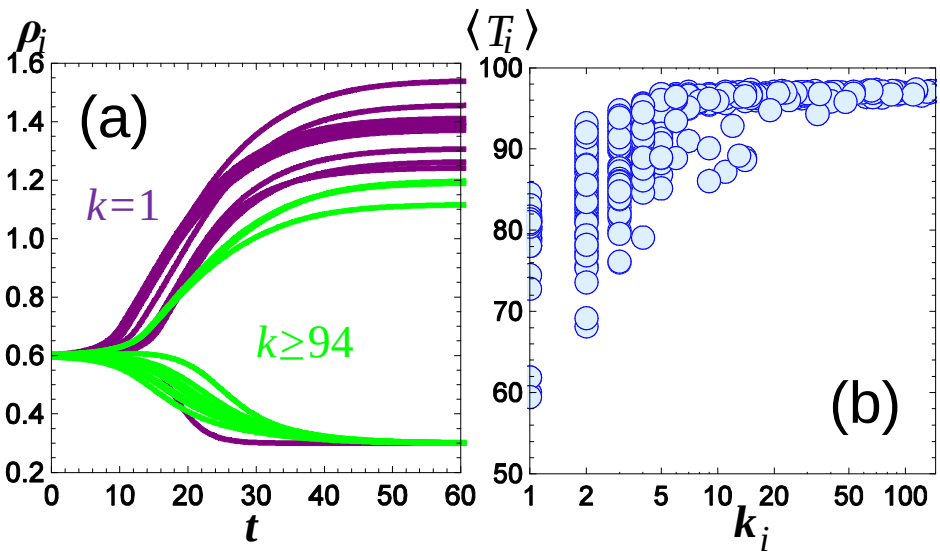


Figure 4.7: (a) Sample time series of density for large ($k \geq 94$) and small ($k = 1$) nodes. (b) Average relaxation time of each node. Each plot corresponds to averaged relaxation time of one node.

### 4.3.5 Influence of delay

In our model, I ignored the effects of delay. In reality, a decrease in aircraft number in an airport is not immediately counted as an increase in the destination airport; that is, there is a time delay, $\tau_{ij}$, required for traveling from airport $i$ to $j$. By including this factor, the system equation is written as

$$\frac{d\rho_i}{dt} = \frac{1}{k_i}\sum_{j=1}^{N} A_{ji} J\left(\rho_j(t-\tau_{ji})\right) - J\left(\rho_i(t)\right). \tag{4.7}$$

The introduction of new parameters $\tau_{ij}$ ($i, j = 1, \cdots, N$), makes the system more inhomogeneous, which may change the properties of final states. Instead of addressing the complicated nature of the equation, here I confirm the delay itself does not change the dynamics presented so far. To exclude the inhomogeneity caused by $\tau_{ij}$, we set $\tau_{ij} = 1$ for every pair of nodes. In addition, I use the random regular network with $k = 12$. The final density distribution in this case is shown

in Fig. 4.8, with the case without delay ($\tau_{ij} = 0$). We cannot see a significant difference between them. Also, I confirmed the stability condition for the uniform stationary state are not influenced by this generalization.

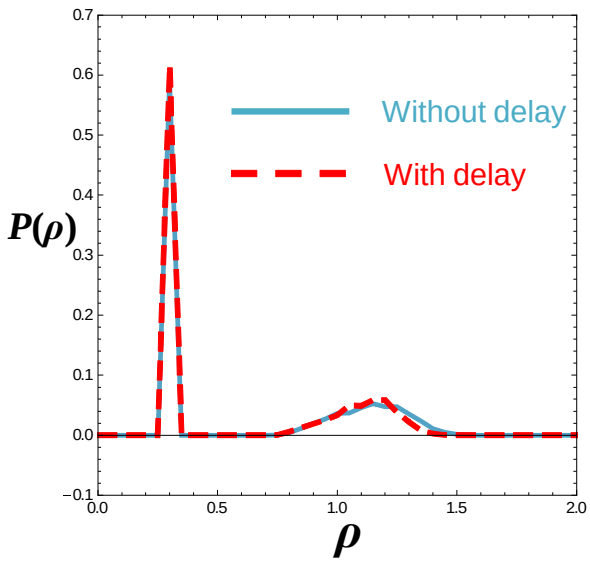


Figure 4.8: Density distribution in the final states for the model Eq. (4.7) with and without the effect of delay. Random regular networks with $k = 12$ were used. The results were averaged over 10 trials. I set $\bar{\rho} = 0.6$. with the uniform delay distribution $\tau_{ij} = 1$ $(i, j = 1, \cdots, N)$.

## 4.4 Summary

We proposed a transportation model for aviation net, focusing on the surface congestion effect. The model exhibits a jamming transition, which is connected to a bifurcation of the system equations. Interestingly, when each component of the network (airport) is jammed, characterized as a negative differential coefficient of a flux-density relationship, the uniform density distribution becomes unstable, decreasing the total network flux (macroscopic jamming). Through relaxation from a uniform to an imbalanced distribution, densities on two neighboring nodes tend to vary inversely, i.e., one increases and the other decreases. However, on a node having large number of links, this correlation vanishes, breaking global correla-

tion structures. In this model, density in a large node changes more slowly than that in a small node because the density inflow to the node is averaged over many nodes and does not change sharply. Note that because the model assumes that the capacity of each node is proportional to its degree, the time constant of the density variation is normalized against the degree. Because of the difference in time coefficient, small nodes are more congested on average. In a small node, however, there may be small traffic demand, which contradicts the assumption that each link has the same amount of traffic. Hence if we take the traffic capacity of links into consideration, the time constant in small nodes is reduced and thus the final density distribution becomes more uniform.

On the other hand, the macroscopic jamming transition presented in this study is not influenced by these simplifications because it is caused by a fundamental bifurcation observed even in a two-component system [8]. In previous studies, this type of jamming transition in air traffic systems has rarely received attention. An effective method to mitigate this jamming is not to accept airplanes beyond the point at which the airport performance decreases. This can be realized by rerouting techniques and the Ground Delay Program (GDP) [1] operated by the Federal Aviation Administration [102–104]. Therefore, knowing the flux–density relationship in each airport for operational reference is vital.

Note that the jamming presented in this study is a completely different phenomenon from the delay propagation phenomena that have been actively studied [86, 94, 102–104]. In these studies, a main cause of delay is the crew and passenger connection disruptions. This type of delay propagates downstream. In this study, congestion in one airport does not simply propagate; it disrupts the density in neighboring airports through its outflow traffic. This study also provides a reason why a small disturbance, for example, due to a bad weather, grows to a large delay from a systemic perspective. Furthermore, note that if a congested airport stops accepting aircraft by following a strategy such as the GDP, congestion propagates to upstream airports. Thus, the propagation direction is determined by its cause.

Our results are based on a model that only considers fixed physical constraints (surface congestion curve) and ignores a flight schedules and operational policies. In future, I intend to address congestion problems on aviation networks more comprehensively by integrating all these factors, which I believe will provide an insight to the problem.

[1] A program that controls departure time of aircrafts on the ground when a destination airport cannot accept them because of bad weather, heavy congestion or an aircraft accident.

# Chapter 5

# Recovery from macroscopic jamming

In the previous chapter, the behavior of transportation systems under the macroscopically jamming state was discussed. Here, I consider the controlling method to mitigate this jamming *after* its occurrence.

## 5.1 Preface

As we have seen in the preceding chapters, the macroscopic jamming reduce the system flux significantly. A simple guaranteed solution to the problem is to increase the effective capacity of the system, which is, however, not always feasible in our society confronted by rapidly increasing demand of traffics. Hence, some external control method is necessary to mitigate the congestion.

In such complex systems, understanding how automatic controls affect their macroscopic features still remains a grand challenge; nevertheless we have to deal with such exigent problems in reality. In this chapter, I consider simple controls, which close nodes adaptively; temporarily remove links led to congested nodes and reconnect them when the congestion is resolved. This type of simple on-off controls are widely adopted, e.g. in traffic light controls [105–107] and ramp metering [105, 108] for vehicular traffic, and the GDP for air traffic [102–104]. We show that this control method could cause a sudden breakdown, which is characterized by a discontinuous phase transition to the *deadlock* state, whereas it is partly effective for alleviating congestion in a certain parameter regime. This deadlock transition stems from the control I adopt, and is a different phenomenon

from previously known deadlock phenomena observed e.g. in BML model [109–111]. By disclosing the dynamics caused by the control, I discuss its effectiveness and criteria for designing a control law on transportation systems.

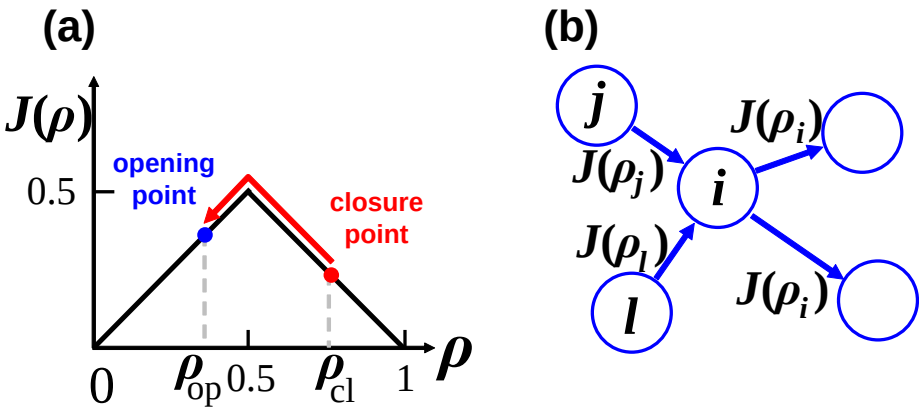


Figure 5.1: (a) flow–density relationship and control points. (b) Inflow to and outflow from a node in the network.

## 5.2 Controlling method

Before defining the controlling rules, I briefly review our model. In this chapter, for simplicity, I assume a piecewise linear flow–density relationship [Fig. 5.1(a)], $J(\rho) = \min\{\rho, 1-\rho\}$, where $\rho \in [0,1]$ and $J$ denote density and flow, respectively.

We consider density distribution on a network of $N$ nodes that are labeled by $i$ (, $j$ and $l$)= $1, \cdots N$. For each density value in node $i$, $\rho_i$, flow on a link from the node is determined by the function value, $J(\rho_i)$. Each node sends and receives density thorough the links [Fig. 5.1(b)] defined by an adjacency matrix $\mathbf{A}$, whose element $A_{ij}$ is 1 if there is a link from node $i$ to $j$, and 0 otherwise. As in the general model defined in Chap. 2, we can introduce the weight $w_{ij}$ if necessary. However, for the sake of clarity of discussion, here I restrict myself to considering unweighted networks. Hence, time development of the density in node $i$ is written as

$$\frac{d\rho_i}{dt} = \sum_{j=1}^{N} A_{ji} J(\rho_j) - \sum_{j=1}^{N} A_{ij} J(\rho_i). \tag{5.1}$$

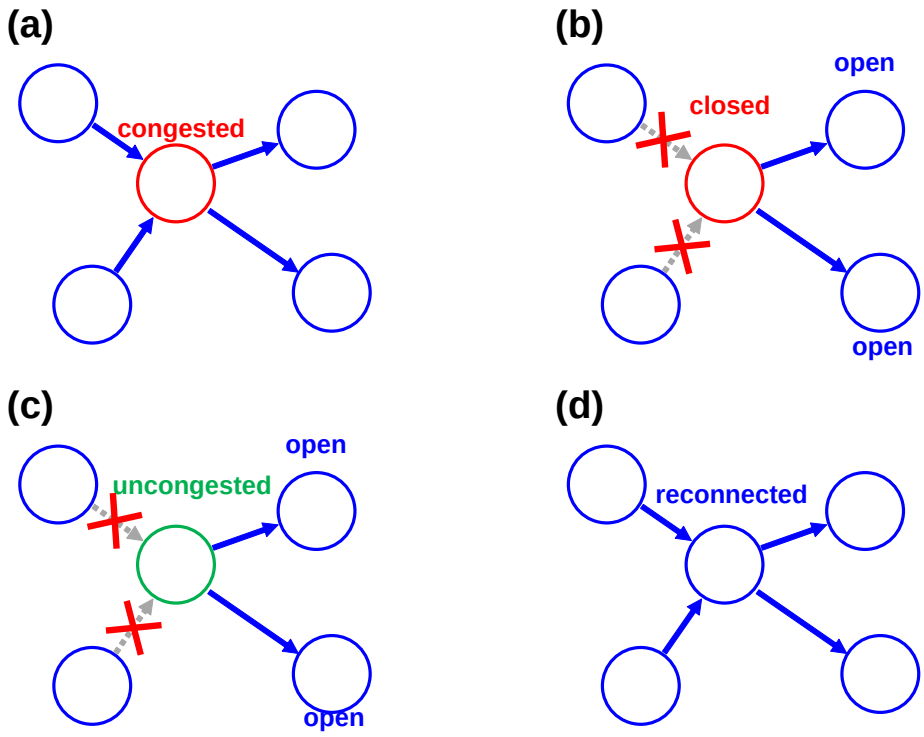


Figure 5.2: Controlling rules. When a node is congested [as in panel (a)], the links leading to the node are disconnected [(b)]. After discharging density to a certain level [(c)], the links are reconnected [(d)].

In this chapter, since we are interested in the nature of the system under control, we ignore individual properties of nodes; the flow–density relationship, capacity and degree of nodes. Moreover, to exclude the effects of network structure, directed random networks with homogeneous in- and out-degrees $k_{\mathrm{in}} = k_{\mathrm{out}} = k$ are used.

As discussed in Sec. 3.3, the system exhibits a macroscopic jamming transition. When the density in a node is in the jamming regime ($\rho > \frac{1}{2}$), small increase in density leads to a decrease of outflow, which causes further congestion. This effect destabilizes uniform flow in networks. Hence, I consider a control method as follows. Since when the density in the system is high, density concentrates in congested nodes, the method must disperse it in some way. As the simplest control, I here consider the following operations: (i) when the density in node $i$ exceeds $\rho_{\mathrm{cl}}$, links leading to the node are disconnected [Fig. 5.2(b)], i.e., $A_{ji} = 1 \to A_{ji} = 0$ ($j \neq i$) (*closed*); (ii) when the density in a closed node drops below $\rho_{\mathrm{op}}$, the incoming links are all reconnected [Fig. 5.2(d); see also Fig. 5.1(a)]. The flow that is supposed to travel the disconnected links must stay in the present node or detour using other links. In this chapter, both rules are studied separately. The first rule is referred to as the *queuing rule*, wherein the canceled flow stays in the departure node, resulting in no change in the system equation for open nodes (5.1), whereas for closed nodes the inflow term vanishes:

$$\frac{d\rho_i}{dt} = \begin{cases} \sum_{j=1}^{N} A_{ji} J(\rho_j) - \sum_{j=1}^{N} A_{ij} J(\rho_i) & (i : \text{open}), \\ -\sum_{j=1}^{N} A_{ij} J(\rho_i). & (i : \text{closed}). \end{cases} \tag{5.2}$$

The second rule is referred to as the *detouring rule*, which diverts the canceled flow equally to open links. Thus, flux to an open node is increased by this extra flow:

$$\frac{d\rho_i}{dt} = \begin{cases} \sum_{j=1}^{N} \frac{kJ(\rho_j)}{\sum_{l=1}^{N} A_{jl}\sigma(l)} - kJ(\rho_i) & (i : \text{open}), \\ -kJ(\rho_i) & (i : \text{closed}), \end{cases} \tag{5.3}$$

where $\sigma(l)$ represents the state of node $l$, i.e., open ($\sigma(l) = 1$) and closed ($\sigma(l) = 0$) states. For closed nodes, the equation is not influenced by the state of neighboring nodes if at least one outgoing link is open. When the destination nodes are all closed, the outflow from a node vanishes, regardless of its state.

### 5.2.1 Stability of stationary flow

Next, we confirm the condition for the macroscopic jamming. Because the random regular network defined in this chapter is a *balanced* network, i.e.,

$$\sum_{j=1}^{N} A_{ji} = \sum_{j=1}^{N} A_{ij} = k, \tag{5.4}$$

we can apply the result in Sec. 3.3. Hence, the macroscopic jamming occurs in the region $\rho > \frac{1}{2}$.

### 5.2.2 Parameter settings

In this chapter we restrict ourselves to considering the case of $\rho_{\mathrm{cl}} = 0.75$, and focus on the system's dependence on $\rho_{\mathrm{op}}$ and the average density, $\overline{\rho} = \frac{\sum_{i=1}^{N} \rho_i}{N}$. We conducted simulations for $N = 100$ and $k = 10$ to compare the results with the predictions obtained by a mean-field theory. Note that the arguments in this chapter is not affected significantly by these specifications (see also Sec. 5.3.5) . The system equations were integrated by using Runge-Kutta method with $dt = 0.0001$. Simulation results were obtained by averaging 10 trials for each condition.

## 5.3 Results

### 5.3.1 Equivalence of the two control rules

In a mean-field treatment, the system equations of the two rules are equivalent through a transformation,

$$\frac{t_{\mathrm{q}}}{x} = t_{\mathrm{d}}, \tag{5.5}$$

where $x = \frac{\sum_{i=1}^{N} \sigma(i)}{N}$ is the ratio of open nodes in the thermodynamic limit. This equivalence is explained as follows.

Here I apply a mean-field approximation to the links of each node as follows. I assume that $k$ directed links starting from each node are composed of $xk$ links ending in open nodes and $(1 - x)k$ links ending in closed nodes. Similarly, $k$ directed links ending in each node are always composed of $xk$ links starting from open nodes and $(1 - x)k$ links starting from closed nodes. In short, connections between links are assumed to be completely randomized, using $x$ being the ratio

of open nodes (Fig. 5.3). Under this assumption, the time development of $\rho_i$ under the queuing rule obeys

$$\frac{d\rho_i}{dt_{\mathrm{q}}} = \begin{cases} -kxJ(\rho_i) & (i\text{: closed}), \\ \sum_{j=1}^{N} A_{ji}J(\rho_j) - kxJ(\rho_i) & (i\text{: open}), \end{cases} \tag{5.6}$$

and under the detouring rule, it obeys

$$\frac{d\rho_i}{dt_{\mathrm{d}}} = \begin{cases} -kJ(\rho_i) & (i\text{: closed}), \\ \frac{\sum_{j=1}^{N} A_{ji}J(\rho_j)}{x} - kJ(\rho_i) & (i\text{: open}), \end{cases} \tag{5.7}$$

where subscripts q and d denote the queuing and detouring rules, respectively. It is straightforward from Eqs. (5.6) and (5.7) that in the mean-field approximation, the queuing and detouring rules result in the identical time development with a scaling transformation, $xt_{\mathrm{q}} = t_{\mathrm{d}}$. Correspondingly, the following relationship holds for average flow rates under the two rules.

$$\frac{\overline{J_{\mathrm{q}}}}{\overline{J_{\mathrm{d}}}} = x. \tag{5.8}$$

Figure 5.4 exhibits the comparison between $\frac{\overline{J_{\mathrm{q}}}}{\overline{J_{\mathrm{d}}}}$ and $x_{\mathrm{q}}$, which should be the same value if the two rules are equivalent. The agreement in the figure shows this equivalence is valid when the degree, $k$, is large.

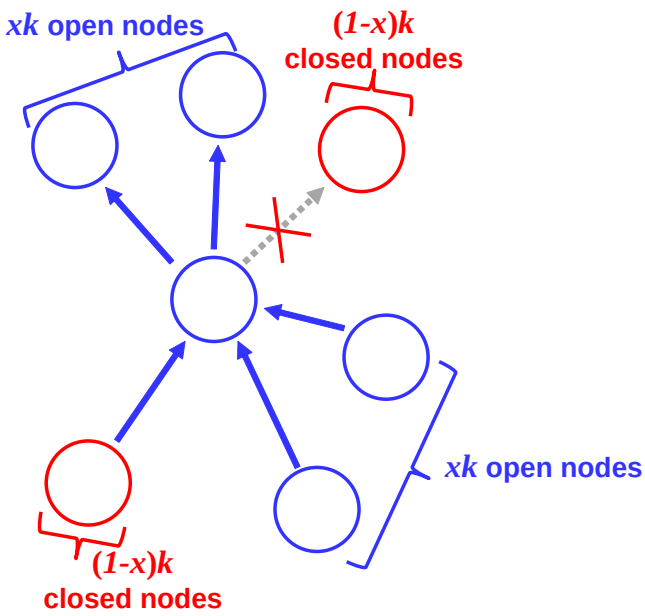


Figure 5.3: Mean-field approximation.

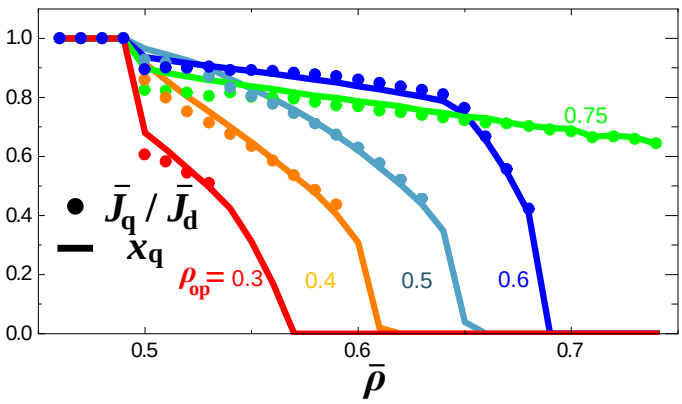


Figure 5.4: Comparison between $\frac{J_q}{J_d}$ and $x_q$. Initial conditions are identical to those of Fig. 4 in the main text.

### 5.3.2 Free-flow, controlled and deadlock phases

First, we focus on the cases of $\rho_{\mathrm{op}} = 0.5$. Depending on the value of the average density, the system exhibits three different phases, i.e., the free-flow, controlled and deadlock phases (Fig. 5.5). These phases are observed in the system both under queuing and detouring operations. When the average density is small, congested nodes do not appear and uniformly distributed flow is achieved [Fig. 5.5(a)]. As the average density increases, congested nodes appear and our control rules apply. Because these operations increase the load in neighboring nodes, congested nodes appear on different locations while the operated node is recovering from the congested state. Thus, a certain ratio of nodes are almost constantly closed, which state is referred to as the controlled phase. When we further increase the average density, all the nodes become closed. In this state, nodes cannot accept nor send density, and thus flow vanishes. Since the node capacity is temporarily limited during node closure, the operations effectively reduce the total capacity of the system.

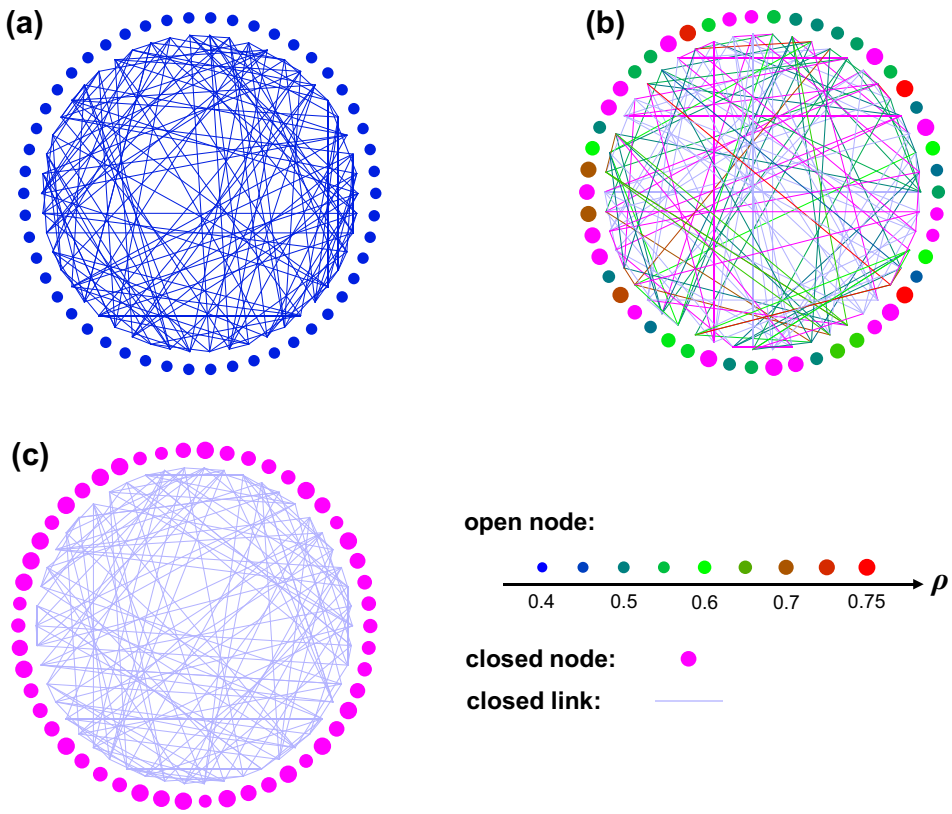


Figure 5.5: Snapshots of (a) free-flow phase ($\bar{\rho} = 0.4$), (b) controlled phase ($\bar{\rho} = 0.55$) and (c) deadlock phase ($\bar{\rho} = 0.65$). Each disk represents a node, whose radius and color correspond to the density value. When a node is closed, the node and disconnected links are expressed by a magenta disk and gray lines, respectively. For display purpose, the networks are generated for $N = 50$ and $k = 3$.

Next, I discuss the phase transitions for various $\rho_{\mathrm{op}}$ values. Fig. 5.6 shows the phase diagram in $\bar{\rho}$–$\rho_{\mathrm{op}}$ plane. Simulation results were obtained by observing the state of the system after 1 000 000 simulation time steps. The initial density distribution in the system was set uniformly, but perturbed with randomly selected 10 closed nodes ($\rho = \rho_{\mathrm{cl}}$). When $\rho_{\mathrm{op}}$ is small, the controlled phase is not observed. In this region, closure time is too large, and thus it adversely affects the system by less utilizing the capacity of the network. For large $\rho_{\mathrm{op}}$ values, the controlled phase exists when the average density is moderately large. Here the control operations

function without causing a breakdown. Because large $\rho_{\rm op}$ values lead to small closure time of controlled nodes, the deadlock phase region shrinks for such $\rho_{\rm op}$ values.

In a practical context, the transition line from the controlled phase to the deadlock phase is important. Since the two rules are equivalent in the mean-field limit, we analyze the detouring rule, in which the time development of density in a closed node is known [Eq.(5.3)]. First, closed nodes in the controlled phase are focused on.

Under the detouring rule, the dynamics in a closed is deterministic. In this state, the density in a closed node decreases as

$$\frac{d\rho_i}{dt} = -kJ(\rho_i). \tag{5.9}$$

Hence, the time required for the density to pass the interval $[\rho, \rho + d\rho]$ is inversely proportional to the absolute value of this equation. Moreover, if node closure takes place temporarily at random, the density distribution of nodes, $Q(\rho)$, are proportional to this time interval,

$$Q(\rho) = T_{\rm cl\to op}\frac{1}{kJ(\rho)}. \tag{5.10}$$

The normalization constant $T_{\rm cl\to op}$ corresponds to the time required for a closed node to open given by

$$\begin{aligned} T_{\rm cl\to op} &= \int_{\rho_{\rm op}}^{\rho_{\rm cl}} \frac{d\rho}{kJ(\rho)} && (5.11)\\ &= \begin{cases} \int_{\rho_{\rm op}}^{\frac{1}{2}} \frac{d\rho}{k\rho} + \int_{\frac{1}{2}}^{\rho_{\rm cl}} \frac{d\rho}{k(1-\rho)} & (\rho_{\rm op} < \frac{1}{2}), \\ \int_{\rho_{\rm op}}^{\rho_{\rm cl}} \frac{1}{k(1-\rho)} & (\rho_{\rm op} \geq \frac{1}{2}), \end{cases} && (5.12)\\ &= \begin{cases} \frac{1}{k}\log\frac{1}{4(1-\rho_{\rm cl})\rho_{\rm op}} & (\rho_{\rm op} < \frac{1}{2}), \\ \frac{1}{k}\log\frac{1-\rho_{\rm op}}{1-\rho_{\rm cl}} & (\rho_{\rm op} \geq \frac{1}{2}). \end{cases} && (5.13) \end{aligned}$$

Using this distribution, the average density in closed nodes is calculated as

$$\begin{aligned} \bar{\rho}_{\rm closed} &= \int_{\rho_{\rm op}}^{\rho_{\rm cl}} \rho Q(\rho) d\rho \\ &= \begin{cases} \frac{\rho_{\rm cl}+\rho_{\rm op}+\log 2(1-\rho_{\rm cl})-1}{\log 4(1-\rho_{\rm cl})\rho_{\rm op}} & (\rho_{\rm op} < \frac{1}{2}), \\ 1 - \frac{\rho_{\rm cl}-\rho_{\rm op}}{\log\frac{1-\rho_{\rm op}}{1-\rho_{\rm cl}}}. & (\rho_{\rm op} \geq \frac{1}{2}). \end{cases} && (5.14) \end{aligned}$$

At the transition point when the deadlock occurs (all the nodes become closed), this value should coincide with the overall average density, i.e., $\bar{\rho} \simeq \bar{\rho}_{\text{closed}}$. This expression is shown in Fig. 5.6, and gives an accurate prediction when $\rho_{\text{op}}$ is large. Because this approximate analysis assumes that the number of closed node continuously increases from the controlled phase to the deadlock phase with increasing average density, the equation cannot describe the transition from the free-flow phase to the deadlock phase. The agreement between this equation and simulation results implies that the closure operations can be regarded to occur almost at random without causing synchronization.

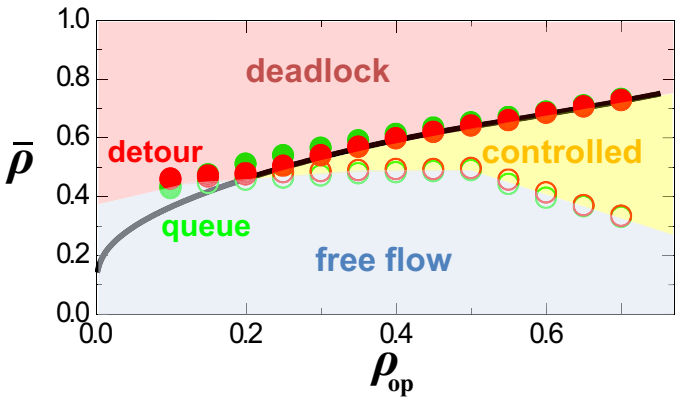


Figure 5.6: Phase diagram of the system. Closed and open circles represent transition points obtained by simulations. Black bold line is the theoretical prediction, Eq. (5.14). Simulation results were obtained by examining the presence of a closed node after sufficiently long time ($t = 200$). At $t = 0$, 10 nodes were selected randomly to be closed with $\rho = 0.75$.

### 5.3.3 Macroscopic flow–density relationship

As the most important performance index of the system, I study a macroscopic relationship between the average flow per link and the average density, which is defined by

$$\bar{J} = \frac{\sum_{i=1}^{N} \sum_{j=1}^{N} A_{ij} J(\rho_i)}{Nk}. \tag{5.15}$$

Figures 5.7(a) and 5.7(b) show the macroscopic flow–density relationship for the queuing rule and detouring rule, respectively. It is convenient for understanding

the results to consider the base line case $\rho_{\mathrm{op}} = \rho_{\mathrm{cl}} = 0.75$, wherein nodes reject inflow only when their (prescribed permissible) capacity ($\rho_{\mathrm{cl}}$) is fully occupied. Because of the system's intrinsic instability, the uniform density distribution is not achieved in the density region $\overline{\rho} > \frac{1}{2}$, in which the macroscopic flow decreases. If the macroscopic flow is larger than that in the base line case, the controls are effective. We can partly see the effectiveness in the controlled phase; however, when the average density further increases, the macroscopic flow sharply drops to zero, which corresponds to the phase transition to the deadlock phase. When $\rho_{\mathrm{op}}$ is small, the closure time is large, and thus the system falls into the deadlock phase even with a low average density. In both rules, the average flow entirely increases with increasing $\rho_{\mathrm{op}}$ when $\rho_{\mathrm{op}} \leq \frac{1}{2}$. As we further increase $\rho_{\mathrm{op}}$, the inclination of $\overline{J}$ becomes gentle, and the controlled phase can be achieved for larger average density. Therefore, from a practical perspective, the most desirable $\rho_{\mathrm{op}}$ depends on $\overline{\rho}$ (and $\rho_{\mathrm{cl}}$).

In contrast with the queuing rule, the detouring rule does not stop flow even if the next node is closed by diverting it to other open nodes. Hence the average flow is larger than that operated under the queuing rule. This relationship is also verified by a scaling transformation between them; $\frac{J_{\mathrm{q}}}{x} = J_{\mathrm{d}}$ [Eq. (5.8)].

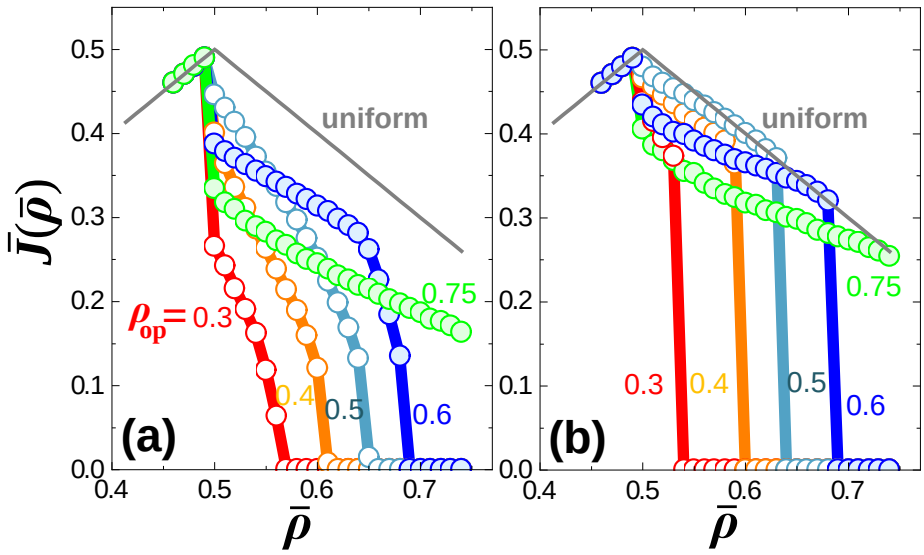


Figure 5.7: Macroscopic flow–density relationship for (a) the queuing rule and (b) the detouring rule. Note that, here the initial density values are set as $\rho_i = \bar{\rho} + \delta_i$, where $\delta_i$ is a small random value drawn from a uniform distribution $[-0.005, 0.005]$.

### 5.3.4 Density separation and control

In the detouring rule, high average flow is achieved in the controlled phase. This can be understood by considering the density distributions of nodes, $P(\rho)$. Figure 5.8 shows the density distributions for $\rho_{\mathrm{op}} = \rho_{\mathrm{cl}} = 0.75$ (the base line case) and $\rho_{\mathrm{op}} = 0.5$. In the base line case, the distribution is bimodal, whose peaks are approximately at $\rho = 0.75$ and 0.4. In this state, once a node becomes congested ($\rho \simeq 0.75$), it cannot escape from the state because the neighboring nodes with small density ($\rho \simeq 0.4$) send more flow to the node than the outflow from the congested node. Thus, this density separation occurs. In contrast, for $\rho_{\mathrm{op}} = 0.5$, the density distribution is unimodal and the density separation is effectively suppressed by the closure operation that helps the density to decrease. Since the flow between nodes takes the highest value in the middle density, collecting the density into the middle contributes to increasing the average flow that is given by integrating $P(\rho)J(\rho)$.

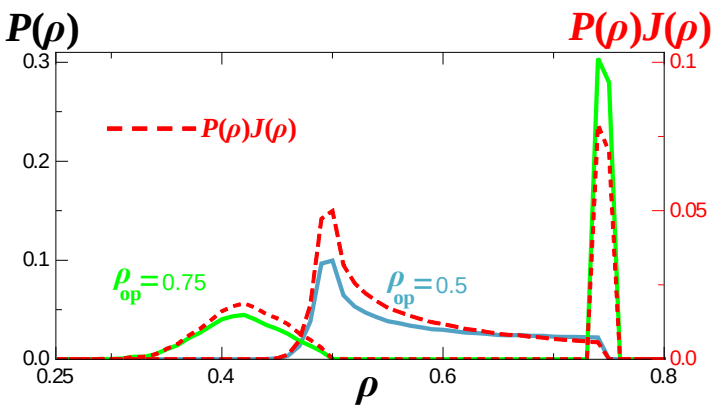


Figure 5.8: Density distribution (solid lines) and flow distribution (red broken lines) in the controlled phase ($\bar{\rho} = 0.6$).

### 5.3.5 Influence of degree $k$ on system dynamics

Figure 5.9 displays flow–density relationship for different degree values, $k$. Difference in $k$ does not influence qualitative characteristics of the system. As $k$ increases the deadlock transition sharpens. When $k$ is small, flow is often completely blocked because of the small number of routes from a node. As a result, the average flux is suppressed, but at the same time, due to the restriction of flow, the deadlock transition occurs at higher density.

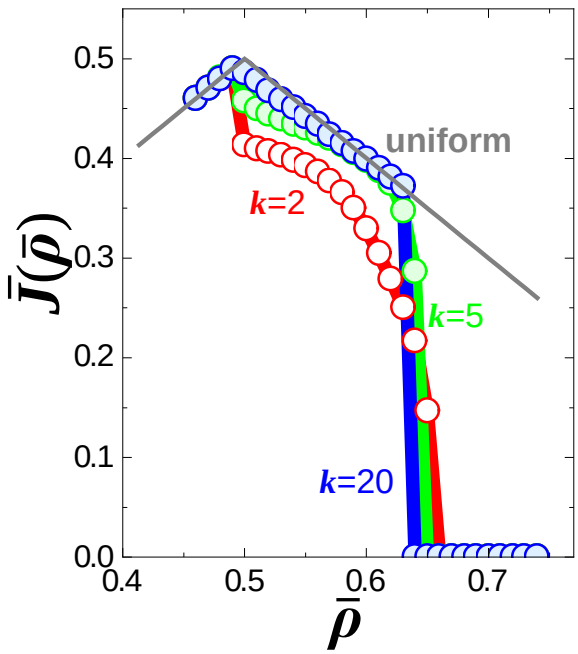


Figure 5.9: flow–density relationship for different degree, $k$. Here I set $\rho_{\mathrm{op}} = 0.5$. Other conditions are identical to those of Fig. 4(b) in the main text.

### 5.3.6 Absence of structural behavior in the controlled phase

As explained in the previous subsection, the average flux is improved by suppressing the density separation. It is natural to consider that this could be also explained by the presence of a structure of closed and open nodes. In this subsection, I discuss the correlation in the states in neighboring two nodes. Because the flow from a node depends on the state in the next nodes, this quantity is the simplest index to examine the presence of the structure.

I define the conditional probability for two nodes connected by a link, $P(c|o)$, as the probability of finding a closed node at the end of a link when the corresponding node in its origin is open. That is, it is equivalent to the probability of finding a link connecting closed and open nodes at its destination and origin ($o \to c$), divided by the probability of finding a open node. If the states in the neighboring nodes are uncorrelated, the conditional probability simply coincides

with the probability of finding a closed node (given by $1 - x$) because the information about the node state at the origin of a link does not influence the state in its destination. Hence, the difference between these two probability shows the degree of correlation and structuralization. From Fig. 5.10, we can conclude that the difference is not significant; and thus, the states of nodes distribute almost at random. This might be due to the absence of structure in the random regular network I adopted.

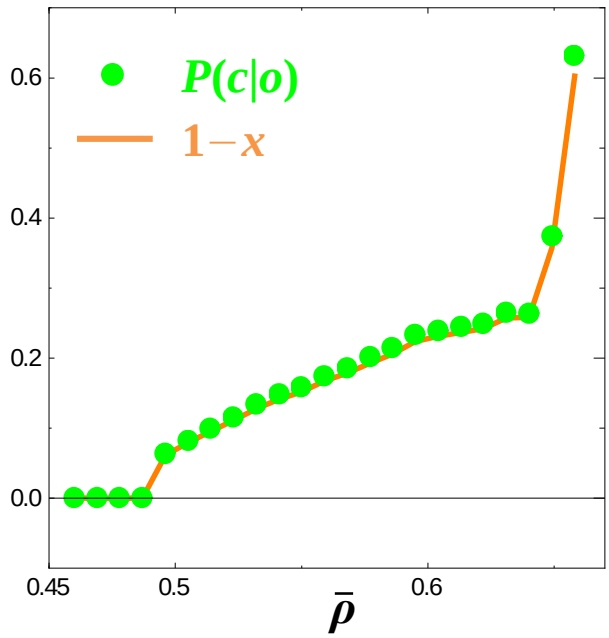


Figure 5.10: The conditional probability, $P(c|o)$ (green disks), and closure probability, $1 - x$ (orange line). I set $\rho_{\mathrm{op}} = 0.6$.

## 5.4 Summary

A simple control method for mitigating congestion on network transport was investigated. We found complex behavior such as the deadlock phase transition, which is crucially important for implementing these rules to reality. The control impedes density separation among nodes, thus enhancing macroscopic per-

formance of the system. However, to prevent deadlock situations, one can see the trade-off relationship between higher flow and small deadlock density. This deadlock phenomenon is similar to gridlocks observed in urban traffic [17] or a more simplified particle model, BML model [109–111], which are caused by physical exclusion of vehicles (particles). In contrast, the deadlock in our model is caused by virtual exclusion of a controlling low. These intuitively understandable findings are useful for designing such control systems.

As expected, the absence of network structure in our study enabled us to analyze and understand the system clearly. On the basic knowledge obtained in this chapter, the effects of network structure in real networks should be investigated in future works. We believe that they will trigger rich varieties of studies such as tolerance [112, 124] of transportation networks, selective protection of nodes [114–117], and the effects of spacial structure in a node [118–120].

# Chapter 6

# Conclusions

In this thesis, a theory of density-dependent transport on networks was presented. Through a simple model, I proved the existence of macroscopic jamming phenomena. It is closely related to a bifurcation in the system equation, and the condition for preventing the jamming was investigated.

This macroscopic jamming is relevant to jamming phenomena in real traffic networks, such as road networks and airport networks. To address this demand imbalance in networks, there are many practical operations. For example, in road traffic, there is a method of reducing traffic demand by charging on use of predefined congested roads [121]. Airport networks also has a control method called the ground delay program [102], which postpones the departure of aircraft when its destination airport is too congested. To capture these operations and facilitate the safe use of them, I considered a simple controlling method in the discussed model. In the control, congested nodes are temporarily closed by removing the links leading to them. Being different from classical approaches applied for linear transportation systems [122], I adopted a physics approach to reveal how an external control affects the nonlinear system dynamics. By this approach, the fundamental behavior of the system was uncovered. The most important fact is that the control is effective for a certain parameter regime, and that a breakdown of the system could be caused by the control. The knowledge about the quantitative feature of the boundary of the two phases is useful for designing a control method.

The results presented in this thesis are not greatly affected by the structure of networks, and instead, their degree distribution is a determinant of the dynamics. This might be due to the fact that the model considered in this thesis is a generalization of diffusion process on networks. Besides the macroscopic jamming transition, the system does not display a singular phenomenon. The time develop-

ment of the system state is directed to a possible stable state, and does not exhibit periodic or chaotic trajectories, when no control is applied. This property enabled us to understand the behavior of the system under a simple control.

In this thesis, I assumed homogeneous systems to capture the essential characteristics of the density-dependent transport. However, real systems are often inhomogeneous in some senses. First, the capacity of the nodes are inhomogeneous, which could give a rise to "key" nodes to prevent and control jamming. The node with the smallest capacity should be payed attention since the system has a vulnerability of a *chain type*; that is, the jamming in the weakest nodes triggers macroscopic imbalance in network flow. When the network has a significant inhomogeneity, for example a scale free structure, its effect might be important. Second, inhomogeneity in delay time (travel time required for traveling from node to node) might affect the system dynamics. As discussed in Sec. 4.3.5, a homogeneous delay in the system does not greatly influence the qualitative characteristics. However, when the delay is inhomogeneous, the system could display oscillatory or chaotic behavior. Third, I assumed homogeneous fundamental diagrams in all nodes. Especially, the critical density that gives a peak in the fundamental diagram is important because above this density, outflow from the node decreases, which leads to further congestion. Moreover, the degree of decrease in the jamming region, $\left.\frac{dJ}{d\rho}\right|_{\rho>\rho_{\mathrm{cr}}}$, is also important since it determines the speed of falling into a breakdown. Finally, considering these types of inhomogeneities, the control defined in Chap. 5 could be optimized. That is, for example, protecting the most influential nodes may better mitigate the jamming. For more simple (linear) network flow models, the *centrality* is known to be a key measure [123], which might be useful also in our case.

The *cascading failure* [124–126] is also worth mentioning in this context. In electrical power grids, when a line is disconnected, the electricity is shifted to neighboring lines, increasing their loads. In these lines, the power exceeds their capacity, which leads to more breakdowns. Through these processes, a large number of lines are broken, which causes a blackout in a macroscopic level. The jamming dynamics presented in this thesis deals with a kind of break down; however, they are essentially different from each other for some reasons. First, in the model in Sec. 4 for air traffic, the node can accept density still after it become congested. Thus, the neighboring nodes do not have to accept extra flow. In fact, negative correlation is observed in the neighboring nodes [as shown in Fig. 4.5(a)]. When a control in Chap. 5 is applied, flow to a congested node is diverted to neighboring nodes. However, being different from power grids, a *broken* node recovers after

some time. Thus, such cascading structure is not formed, as explained in Sec. 5.3.6.

In future works, more practical studies using empirical data (, which is not accessible at the moment) would yields fruitful results for better designing and controlling density-dependent traffics on networks.

# References

[1] *Nonlinear Dynamics of Production Systems*, edited by G. Radons and R. Neugebauer (Wiley, NewYork; 2003).

[2] D. Helbing, New J. Phys. **5**, 90.1 (2003).

[3] D. Helbing, S. Lämmer and T. Sneidel, Phys. Rev. E **70**, 066116 (2004).

[4] R. Albert, H. Jeong and A. -L. Barabási, Nature (London) **401**, 130 (1999).

[5] B. A. Huberman and L. A. Adamic, Nature (London) **401**, 131 (1999).

[6] C. F. Daganzo, Transp. Res. B **28**, 269 (1994).

[7] C. F. Daganzo, Transp. Res. B **29**, 79 (1995).

[8] C. F. Daganzo, V. V. Gayah and E. J. Gonzales, Transp. Res. B **45**, 278 (2011).

[9] J. Esser and M. Schreckenberg, Int. J. Mod. Phys. C **8**, 1025 (1997).

[10] D. Helbing, S. Lämmer and J.-P. Lebacque, in *Optimal control and dynamic games* (Springer US, 2005), p. 239.

[11] M. Gugat, M. Herty, A. Klar and G. Leugering, J. Optim. Theor. Appl. **126**, 589 (2005).

[12] W. Li and X. Cai, Phys. Rev. E **69**, 046106 (2004).

[13] R. Guimerà and L. A. N. Amaral, Eur. Phys. J. B **38**, 381 (2004).

[14] R. Guimerà, S. Mossa, A. Turtschi and L. A. N. Amaral, Proc. Nat. Acad. Sci. **102**, 7794 (2005).

[15] G. Bagler, Physica A **387**, 2972 (2007).

[16] M. Zanin and F. Lillo, Eur. Phys. J. Special Topics **215**, 5 (2013).

[17] C. F. Daganzo, Transp. Res. B **41**, 49 (2007).

[18] H. S. Mahmassani and M. Saberi, Procedia Soc. Behav. Sci. **80**, 79 (2013).

[19] J.-F. Zheng, Z.-Y. Gao and X.-M. Zhao, Physica A **385**, 700 (2007).

[20] I. Simonsen, L. Buzna, K. Peters, S. Bornholdt and D. Helbing, Phys. Rev. Lett. **100**, 218701 (2008).

[21] Road Transport Bureau, Ministry of Land, Infrastructure and Transport, Japan. URL: http://www.mlit.go.jp/road/ir/ir-perform/h19/02.pdf (accessed in January 2015; Japanese).

[22] D. Helbing, Rev. Mod. Phys. **73**, 1067 (2001).

[23] T. Nagatani, Phys. Rep. **65**, 1331 (2002).

[24] Map generated by Google map. URL: https://www.google.co.jp/maps/@35.7100405,139.6521165,12z/data=!5m1!1e1?hl=en (accessed in January 2015).

[25] B. D. Greenshields, in *Proceedings of the Highway Research Board* (Highway Research Board, Washington, D. C.), vol. 14, p. 448 (1935).

[26] F. L. Hall, B. L. Allen and M. A. Gunter, Transp. Res. A **20**, 197 (1986).

[27] L. A. Pipes, Transp. Res. **1**, 21 (1967).

[28] M. Bando, K. Hasebe, A. Nakayama, A. Shibata and Y. Sugiyama, Phys. Rev. E **51**, 1035 (1995).

[29] S. Krauss, P. Wagner and C. Gawron, Phys. Rev. E **55**, 5597 (1997).

[30] H. Lenz, C. K. Wagner and R. Sollacher, Eur. Phys. B **7**, 331 (1999).

[31] E. Tomer, L. Safonov and S. Havlin, Phys. Rev. Lett. **84**, 382 (2000).

[32] M. Treiber, A. Hennecke and D. Helbing, Phys. Rev. Lett. **62**, 1805 (2000).

[33] M. Cremer and J. Ludwig, Math. Comput. Simul. **28**, 297 (1986).

[34] K. Nagel and M. Shreckenberg, J. Phys. I **2**, 2221 (1992).

[35] O. Biham, A. A. Middleton and D. Levine, Phys. Rev. A **46**, R6124 (1992).

[36] U. Weidmann, *Transporttechnik der fussgänger* (IVT, Institut für Verkehrsplanung, Transporttechnik, Strassen-und Eisenbahnbau; 1993).

[37] A. Seyfried, B. Steffen, W. Klingsch and M. Boltes, J. Stat. Mech. (2005) P10002.

[38] S. P. Hoogendoorn and W. Daamen, Transport. Sci. **39**, 0147 (2005) .

[39] T. Kretz, A. Grünebohm and M. Schreckenberg, J. Stat. Mech. (2006) P10014.

[40] A. Seyfried, O. Passon, B. Steffen, M. Boltes, T. Rupprecht and W. Klingsch, Transport. Sci. **43**, 395 (2009).

[41] J. Zhang, W. Klingsch, A. Schadschneider and A. Seyfried, J. Stat. Mech. (2011) P06004.

[42] A. Jelić, C. Appert-Rolland, S. Lemercier and J. Pettré, Phys. Rev. E **85**, 036111 (2012).

[43] M. Bukáček, P. Harabák and M. Krbálek, in: M. Chraibi, M. Boltes, A. Schadschneider and A. Seyfried eds. *Traffic and Granular Flow '13* (Springer, Berlin; 2015), 93.

[44] D. Helbing, A. Johansson and H. Z. Al-Abideen, Phys. Rev. E **75**, 046109 (2007).

[45] A. Johansson, D. Helbing and P. K. Shukla, Adv. Complex Syst. **10**, 271 (2007).

[46] D. Helbing, I. Farkas and T. Vicsec, Nature **407**, 487 (2000).

[47] A. Seyfried, B. Steffen and T. Lippert, Physica A **368**, 232 (2006).

[48] M. Chraibi, A. Seyfried and A. Schadschneider, Phys. Rev. E **82**, 046111 (2010).

[49] R. Löhner, Appl. Math. Model. **34**, 366 (2010).

[50] M. Moussaïd, D. Helbing and G. Theraulaz, Proc. Natl. Acad. Sci. USA **108**, 6884 (2011).

[51] K. Nishinari, D. Chowdhury and A. Schadschneider, Phys. Rev. E **67**, 036120 (2003).

[52] A. John, A. Schadschneider, D. Chowdhury and K. Nishinari, J. Theor. Biol. **231**, 279 (2004).

[53] A. John, A. Schadschneider, D. Chowdhury and K. Nishinari, Phys. Rev. Lett. **102**, 108001 (2009).

[54] H. Idris, J. Clarke, R. Bhuva and L. Kang, Air Traffic Control Quarterly **10**, 1 (2001).

[55] I. Simaiakis and H. Balakrishnan, Transport. Res. Rec. **2184**, 22 (2010).

[56] B. Derrida, Phys. Rep. **301**, 65 (1998).

[57] A. Schadschneider, Physica A **313**, 153 (2002).

[58] T. J. Ayres, L. Li, D. Schleuning and D. Young, *Fourth International IEEE Conference on Intelligent Transportation Systems*, 826 (2001).

[59] A. Johansson, Phys. Rev. E **80**, 026120 (2009).

[60] I. Karamouzas, B. Skinner and S. J. Guy, Phys. Rev. Lett **113**, 238701 (2014).

[61] M. Takayasu, K. Fukuda and H. Takayasu, Physica A **274**, 140 (1999).

[62] M. Takayasu, H. Takayasu and K. Fukuda, Physica A **277**, 248 (2000).

[63] R. V. Solé and S. Valverde, Physica A **289**, 595 (2001).

[64] M. Laumanns and E. Lefeber, Physica A **363**, 24 (2006).

[65] D. Helbing, S. Lämmer, T. Seidel, P. Šeba and T. Płatkowski, Phys. Rev. E **70**, 066116.

[66] D. Bertsimas and S. S. Patterson, Transp. Sci. **34**, 239 (2000).

[67] D. Helbing, J. Phys. A **36**, L593 (2003).

[68] R. Pastor-Satorras and A. Vespignani, Phys. Rev. Lett. **86**, 3200 (2001).

[69] M. Boguñá and R. Pastor-Satorras, Phys. Rev. E **66**, 047104 (2002).

[70] M. Asano, A. Smalee, M. Kuwahara and S. Tanaka, Transport. Res. Rec. **2039**, 42 (2007).

[71] F. S. Hönseler, M. Bierlaire, B. Farooq, T. Mühlematter, Transp. Res. B **69**, 60 (2014).

[72] I. Simonsen, Physica A **357**, 317 (2005).

[73] C. D. Mayer, *Matrix Analysis and applied linear algebra* (SIAM, 2000).

[74] D. Helbing, I. Farkas and T. Vicsek, Nature (London) **407**, 487 (2000).

[75] D. Helbing, A. Johansson, J. Mathiesen, M. H. Jensen and A. Hansen, Phys. Rev. Lett. **97**, 168001 (2006).

[76] T. Ezaki, D. Yanagisawa and K. Nishinari, Phys. Rev. E **86**, 026118 (2012).

[77] R. Geraerts and M. H. Overmars, Compt. Animat. Virt. W. **18**, 107 (2007).

[78] C. Xie, D. Y. Lin and S. T. Waller, Transp. Res. E **46**, 295 (2010).

[79] Z. Fang, X. Zong, Q. Li, Q. Li and S. Xiong, J. Transp. Geogr. **19**, 443 (2011).

[80] U. Kemloh, A. Seyfried and S. Holl, Adv. Complex Syst. **15**, 1250029 (2012).

[81] F. Alonso-Marroquin, S. I. Azeezullah, S. A. Galindo-Torres and L. M. Olsen-Kettle, Phys. Rev. E (R) **85**, 020301 (2012).

[82] D. Helbing, L. Bunza, A. Johansson and T. Werner, Transp. Sci. **39**, 1 (2005).

[83] J. Filar, P. Manyem and K. White, Ann. Oper. Res. **108**, 315 (2001).

[84] C. Barnhart, P. Belobaba and A. R. Odoni, Transport. Sci. **37**, 368 (2003).

[85] R. de Neufville, A. Odoni, *Airport Systems: Planning, Design and Management.* (McGraw-Hill, New York; 2003).

[86] S. Ahmadbeygi, A. Cohn, Y. Guan and P. Belobaba, J. Air. Transp. Manag. **14**, 221 (2008).

[87] J. Clausen, A. Larsen, J. Larsen and N. J. Rezanova, Comput. Oper. Res. **37**, 809 (2010).

[88] O. Lordan, J. M Sallan and P. Simo, J. Transp. Geogr. **37**, 112 (2014).

[89] J. D. Petersen, G. Sölveling, J. Clarke, E. L. Johnson and S. Shebalov, Transport. Sci. **46**, 482 (2012).

[90] D. Bertsimas and S. S. Patterson, Transport. Sci. **34**, 239 (2000).

[91] P. K. Menon, G. D. Sweriduk and K. D. Bilimoria, J. Guid. Control Dynam. **27**, 737 (2004).

[92] B. Sridhar, T. Soni, K. Sheth and G. B. Chatterji, J. Guid. Control Dynam. **29**, 992 (2006).

[93] L. Lacasa, M. Cea and M. Massimiliano, Physica A **388**, 3948 (2009).

[94] P. Fleurquin, J. Ramasco and V. M. Eguiluz, Sci. Rep. **3**, 1159 (2013).

[95] S. H. Strogatz, Nature **410**, 268 (2001).

[96] R. Albert and A. Barabási, Rev. Mod. Phys. **74**, 47 (2002).

[97] M. E. J. Newman, SIAM Rev. **45**, 167 (2003).

[98] S. Boccaletti, V. Latora, Y. Moreno, M. Chavez and D. -U. Hwang, Phys. Rep. **424**, 175 (2006).

[99] D. Sun and A. M. Bayen, J. Guid. Control Dynam. **31**, 616 (2008).

[100] V. Colizza, R. Pastor-Satorras and A. Vespignani, Nat. Phys. **3**, 276 (2007).

[101] R. M. May, Nature **261**, 459 (1976).

[102] S. Luo and G. Yu, Transport. Sci. **31**, 298 (1997).

[103] J. M. Rosenberger, E. L. Johnson and G. L. Nemhauser, Transport. Sci. **37**, 408 (2003).

[104] S. Lan, J. Clarke and C. Barnhart, Tranport. Sci. **40**, 15 (2006).

[105] M. Papageorgiou, C. Diakaki, V. Dinopoulou, A. Kotsialos and Y. Wang, Proc. IEEE **91**, 2043 (2003).

[106] S. Lämmer and D. Helbing, J. Stat. Mech.: Theor. Exp. (2008) P04019.

[107] A. Schadschneider, D. Chowdhury and K. Nishinari, *Stochastic transport in complex systems: From molecules to vehicles* (Elsevier, New York, 2010).

[108] M. Papageorgiou and A. Kotsialos, in IEEE Proc. Intell. Transp. Syst., pp. 228–239 (2000).

[109] O. Biham, A. A. Middleton and D. Levine, Phys. Rev. A **46**, (R)6124 (1992).

[110] S. Tadaki and M Kikuchi, Phys. Rev. E **50**, 4564 (1994).

[111] S. Tadaki, Phys. Rev. E **54**, 2409 (1996).

[112] R. Albert, H. Jeong and A. -L. Barabási, Nature (London) **406**, 378 (2000).

[113] P. Crucitti, V. Latora, M. Marchiori and A. Rapisarda, Physica A **340**, 388 (2004).

[114] R. Cohen, S. Havlin and D. ben-Avraham, Phys. Rev. Lett. **91**, 247901 (2003).

[115] P. Holme, Eur. Phys. Lett. **68**, 908 (2004).

[116] N. Masuda, New J. Phys. **11**, 123018 (2009).

[117] T. Takaguchi, T. Hasegawa and Y. Yoshida, Phys. Rev. E **90**, 012807 (2014).

[118] I. Neri, N. Kern and A. Parmeggiani, Phys. Rev. Lett. **107**, 068702 (2011).

[119] T. Ezaki and K. Nishinari, J. Stat. Mech.: Theor. Exp. P11002 (2012).

[120] L. Zhang, J. de Gier and T. M. Garoni, Physica A **401**, 82 (2014).

[121] H. Yang and H. J. Huang, *Mahtematical and economic Theory of Road Pricing*, (Elsevier, Oxford; 2005).

[122] T.L. Friesz, L. Luque, R. L. Tobin and B. -W. Wie, Oper. Res. **37**, 893 (1989).

[123] S. P. Borgatti, Physica A **27**, 55 (2005).

[124] P. Crucitti, V. Latora and M. Marchiori, Phys. Rev. E **69**, 045104 (2004).

[125] I. Dobson, B. A. Carreras and D. E. Newman, Chaos **17**, 026103 (2007).

[126] W. -X. Wang and G. Chen, Phys. Rev. E **77**, 026101 (2008).

# Acknowledgment

I would like to express my deepest gratitude to my adviser Prof. Katsuhiro Nishinari whose enormous support and insightful comments were invaluable during the course of my study. I would also like to thank my dissertation committee members: Prof. Kenichi Rinoie, Prof.KojiroSuzuki, Prof. Susumu Shirayama, Prof. Ralph Willox and Prof. Daichi Yanagisawa for their valuable feedback on this dissertation.

I have been blessed with a friendly and cheerful students in the same research group. In particular, Dr. Daichi Yanagisawa and Dr. Ryosuke Nishi offered much advise on my studies for several years, even after their graduation. I am truly indebted and thankful to them.

I would like to express my gratitude to JSPS Research Fellowship for Young Scientists for their financial support.

Finally, I would like to thank my family for everything.